

Impact of Channel Aging on Reconfigurable Intelligent Surface Aided Massive MIMO Systems with Statistical CSI

Anastasios Papazafeiropoulos, Ioannis Krikidis, Pandelis Kourtessis

Abstract—The incorporation of reconfigurable intelligent surface (RIS) into massive multiple-input-multiple-output (mMIMO) systems can unleash the potential of next-generation networks by improving the performance of user equipments (UEs) in service dead zones. However, their requirement for accurate channel state information (CSI) is critical, and especially, applications with UE mobility that induce channel aging make challenging the achievement of adequate quality of service. Hence, in this work, we investigate the impact of channel aging on the performance of RIS-assisted mMIMO systems under both spatial correlation and imperfect CSI conditions. Specifically, by accounting for channel aging during both uplink training and downlink data transmission phases, we first perform minimum mean square error (MMSE) channel estimation to obtain the UE effective channels with low overhead similar to conventional systems without RIS. Next, we derive the downlink achievable sum spectral efficiency (SE) with regularized zero-forcing (RZF) precoding in closed-form being dependent only on large-scale statistics by using the deterministic equivalent (DE) analysis. Subsequently, we present the attractive optimization of the achievable sum SE with respect to the phase shifts and the total transmit power that can be performed every several coherence intervals due to the slow variation of the large-scale statistics. Numerical results validate the analytical expressions and demonstrate the performance while allowing the extraction of insightful design conclusions for common scenarios including UE mobility. In particular, channel aging degrades the performance but its impact can be controlled by choosing appropriately the frame duration or by increasing the number of RIS elements.

Index Terms—Reconfigurable intelligent surface (RIS), channel aging, channel estimation, achievable spectral efficiency, beyond 5G networks.

I. INTRODUCTION

Emerging applications bring challenges that demand ever-higher data rates and increased connectivity/coverage together with ultra-reliable and low-latency wireless communication (URLLC) requirements. Especially, these applications have

led to the development of disruptive technologies such as massive multiple-input multiple-output (mMIMO) systems and millimeter-wave (mmWave) communications [1]. Unfortunately, existing techniques incur additional power and hardware costs while they cannot guarantee an adequate quality of service (QoS) in dead zones due to obstacles. For example, mMIMO exhibits poor performance in low scattering conditions, and the large number of active elements might result in prohibitive energy usage. In particular, they focus on improvements regarding the transmission and reception, while the wireless propagation environment is left uncontrollable. Furthermore, the time-varying and random nature of the wireless channel constitute the ultimate impediment to achieving the URLLC and rate targets.

In this direction, sixth generation (6G) networks, aiming at covering the higher rate demands and more stringent constraints, have appeared with the reconfigurable intelligent surface (RIS) being among its proposed promising technologies. Actually, RIS has attracted significant attention since it overcomes the aforementioned issues [2]–[13]. Specifically, a RIS is a software-defined surface that is usually attached to existing infrastructure to alleviate blockage effects. It consists of a large number of individually-controlled, low-cost, and nearly passive elements. A RIS achieves to adapt to changes in the propagation environment and modify the radio waves since each of its elements can induce an adjustable phase shift to each incident signal, which enables a dynamic control over the wireless propagation channel. For instance, in [3], a minimization of the transmit power at the base station (BS) with signal-to-interference-plus-noise ratio (SINR) constraints took place in a RIS-assisted multi-user (MU) multiple-input single-output (MISO) communication system by jointly optimizing the precoding and reflecting beamforming matrices (RBMs). In [4], the sum rate was maximized subject to a transmit power constraint, while in [5], the sum rate was optimized by accounting also for correlated Rayleigh fading and inevitable hardware impairments at both the transceiver and the RIS. Similarly, in [6], the maximization of the minimum UE rate was studied in the case of a large number of antennas, in [7], the impact of hardware impairments was evaluated, and in [11], the impact of imperfect CSI on the outage probability was investigated. Notably, given that RIS-assisted MIMO systems, having a reduced number of active radio frequency (RF) chains, can achieve similar performance to mMIMO without RIS [13], it is indicated that a more cost and energy-efficient implementation of mMIMO is possible.

A. Papazafeiropoulos is with the Communications and Intelligent Systems Research Group, University of Hertfordshire, Hatfield AL10 9AB, U. K., and with the SnT at the University of Luxembourg, Luxembourg. I. Krikidis is with the IRIDA Research Centre for Communication Technologies, Department of Electrical and Computer Engineering, University of Cyprus, Cyprus. P. Kourtessis is with the Communications and Intelligent Systems Research Group, University of Hertfordshire, Hatfield AL10 9AB, U. K. A. Papazafeiropoulos was supported by the University of Hertfordshire's 5-year Vice Chancellor's Research Fellowship. Also, this work was co-funded by the European Regional Development Fund and the Republic of Cyprus through the Research and Innovation Foundation under the project INFRAS-STRUCTURES/1216/0017 (IRIDA). It has also received funding from the European Research Council (ERC) under the European Union's Horizon 2020 research and innovation programme (Grant agreement No. 819819). E-mails: tapapazaf@gmail.com, krikidis.ioannis@ucy.ac.cy, p.kourtessis@herts.ac.uk.

To reap the benefits of RIS and mMIMO and arrive at realistic conclusions, the acquisition of accurate channel state information (CSI) is of paramount importance [8], [14]–[18].¹ However, channel estimation (CE) in RIS-aided systems is quite challenging because of two main reasons. First, although its passive elements render RIS energy-efficient, they make infeasible conventional CE through transmitting and receiving pilots, which require active elements. Second, RIS generally includes a large number of elements, which require a prohibitively high training overhead that severely reduces the achievable rate. For instance, in [14], an ON/OFF CE scheme was proposed, where the least-squares estimates of all RIS-assisted MISO channels with a single user were calculated one by one. Moreover, other works such as [8], [15] do not provide analytical expressions for the estimated channel that could be exploited for the derivation of the spectral efficiency (SE). In [16], all RIS elements were assumed active during training but a number of sub-phases equal at least to the number of RIS elements are required, which results in a lower rate because the overhead on the coherence time for CE is larger. Moreover, this method does not provide the covariance of the estimated channel vector from all RIS elements to a specific UE but estimates of the individual channels while leaving the correlation among them unknown. An effective method with low overhead compared to previous works is to estimate the cascaded BS-RIS-UE channel in a single phase based on minimum mean square error (MMSE) as in [5]. Notably, another method, which reduces the overhead has been presented by exploiting RIS partitioning into subgroups, e.g., see [18]. Also, therein, an insightful categorization of the various CE approaches concerning RIS-assisted systems has been provided.

In practice, CSI is not only imperfect but can also be outdated because of channel aging [19]–[23]. The cause of channel aging is the UE mobility, which renders the channel time-varying, i.e., contrary to the standard block fading model, the channel evolves with time and is different during each symbol. Thus, a mismatch appears between the current channel and the estimated channel used for detection or precoding. Interestingly, in [22], channel aging was also considered during the training phase for a more realistic study. Several works have studied the impact of channel aging in mMIMO systems as mentioned but little attention has been given to its effect in RIS-assisted systems despite its great significance [23].

In principle, the phase shifts optimization lies on two methodologies with respect to CSI, namely, instantaneous CSI (I-CSI) [3], [4] and statistical CSI (S-CSI) [5], [6], [23]–[29]. The first approach suggests the optimization of the phases at every coherence interval because the related expressions depend on small-scale fading, while the second approach concerns expressions that depend on large-scale statistics, which vary every several coherence intervals. Hence, the latter approach enables considerably the reduction of the signal overhead and the computational complexity, which can

become excessively high in the case of a large number of RIS elements and BS antennas. Moreover, for the same reasons, the S-CSI approach is more energy-efficient. Notably, in high mobility scenarios, which are faster time-varying, the I-CSI method would be very challenging to be implemented since the tuning of the RIS parameters should be repeated very frequently. On the contrary, the application of the S-CSI appears to be more practical.

A. Motivation/Contributions

Faced with these challenges, the motivation of this work is to conduct a realistic characterization of the downlink achievable sum SE of RIS-assisted mMIMO systems accounting for UE mobility and imperfect CSI under correlated Rayleigh fading conditions, when regularized zero-forcing (RZF) precoding is applied.

- Contrary to the majority of existing works on RIS-assisted systems such as [3]–[6], [17], [18], [24]–[28], which considered static UEs, we account for channel aging due to UE mobility. To the best of our knowledge, the only previous works considering channel aging are [23] and [29]. The former focused on mmWave communications with LoS links and with a finite number of BS antennas, while we consider mMIMO systems, correlated Rayleigh fading, and channel aging during the training phase too. The latter did not account for correlated fading mMIMO, and ZF precoding, while we have taken correlation into account and we have focused on mMIMO. Note that no optimization took place in [29]. In addition, we have resorted to the deterministic equivalent analysis to provide the rate for RZF. Also, despite that many previous works have relied on independent Rayleigh fading e.g., [3], [4], we consider correlated Rayleigh fading [30], which appears unavoidable in practice. Moreover, we account for S-CSI instead of I-CSI since the former is more suitable for studying time-varying channels. In particular, compared to other works, which are based on statistical CSI such as [5], [6], [23]–[29], our work is the only one that has studied the impact of channel aging by taking into account correlated fading, imperfect CSI, and RZF being a more advanced precoder, which increases the difficulty for the derivation of closed-form expressions. For example, compared to [5] focusing on the uplink and maximal ratio combining (MRC), we have assumed a more suitable model for RIS correlation, the downlink, RZF, and we have focused on the impact of channel aging. Similarly, compared to [6], we have assumed imperfect CSI, have focused on the sum rate instead of the max-min rate, and have studied channel aging. Also, although channel aging has been studied in [29], no correlation has been considered, ZF instead of RZF has been applied, and no optimization has been performed.
- We introduce channel aging not only in the downlink data transmission phase but also during the uplink training phase as in [22]. In particular, based on [5], we perform MMSE estimation and obtain the effective channel estimate that ages with time. The proposed approach

¹Note that many previous works assumed perfect CSI, which is a highly unrealistic assumption.

provides the estimated channel with low overhead and in closed-form that enables further manipulations to derive the achievable SE. Previous works, e.g., [8], [15] do not provide analytical expressions or have other disadvantages such as high overhead and unknown inter-element correlation [16].

- Exploiting the deterministic equivalent (DE) analysis, we obtain the DE of the downlink sum SE of RIS-assisted mMIMO systems with RZF precoding under UE mobility and correlated Rayleigh fading conditions. The DE results are of great importance because they provide closed-form expressions in terms of a convergent system of fixed-point equations that allow efficient optimization.
- We formulate the maximization problem regarding the sum SE with respect to RBM and total transmit power constraints. Notably, given that the sum SE depends only on large-scale statistics, the proposed optimization can be performed every several coherence intervals, and thus, reduce significantly the signal overhead, which is large in time-varying channels.
- We verify the analytical results with Monte Carlo (MC) simulations, and we shed light on the impact of channel aging on the downlink sum SE of a RIS-assisted mMIMO system due to correlated fading and channel aging. For comparison, we depict results corresponding to no mobility to show the degradation due to channel aging and the inferior performance of maximum ratio transmission (MRT) precoding.

B. Paper Outline

The remainder of this paper is organized as follows. Section II presents the system model of a RIS-assisted mMIMO system with imperfect CSI under correlated Rayleigh fading and channel aging conditions. Section III describes the CE accounting for channel aging. Section IV presents the downlink sum SE, while Section V provides the optimization regarding the RBM and the transmit power. The numerical results are discussed in Section VI, and Section VII concludes the paper.

C. Notation

Vectors and matrices are denoted by boldface lower and upper case symbols, respectively. The notations $(\cdot)^T$, $(\cdot)^H$, and $\text{tr}(\cdot)$ represent the transpose, Hermitian transpose, and trace operators, respectively. The expectation operator is denoted by $\mathbb{E}[\cdot]$ while $\text{diag}(\mathbf{a})$ represents an $n \times n$ diagonal matrix with diagonal elements being the elements of vector \mathbf{a} . Also, the notations $\xrightarrow[M \rightarrow \infty]{\text{a.s.}}$ and $a_n \asymp b_n$ with a_n and b_n being two infinite sequences denote almost sure convergence as $M \rightarrow \infty$. The notation $\lim_{x \rightarrow c} f(x)$ denotes the limit of f of x as x approaches c , and the notation $\frac{\partial f(x)}{\partial x}$ denotes the partial derivative of f with respect to x . Finally, $\mathbf{b} \sim \mathcal{CN}(\mathbf{0}, \Sigma)$ represents a circularly symmetric complex Gaussian vector with zero mean and covariance matrix Σ .

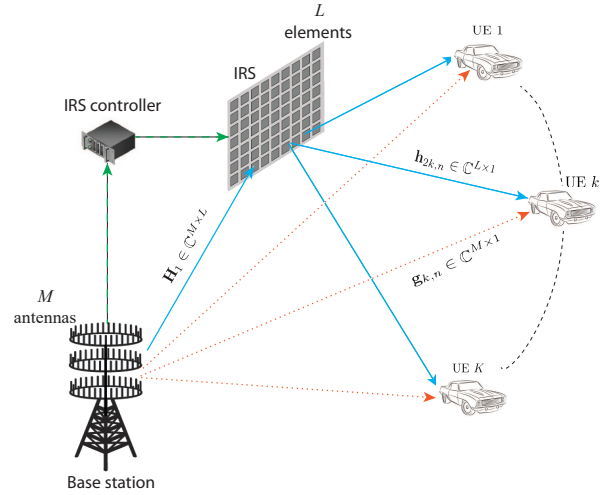


Fig. 1. A downlink RIS-assisted mMIMO communication system with M BS antennas, L RIS elements, and moving K UEs.

II. SYSTEM MODEL

We consider a RIS-assisted downlink mMIMO system, where a BS, equipped with M antennas communicates with K single-antenna noncooperative UEs behind obstacles. A RIS, consisting of L passive reflecting elements is located in the LoS of the BS to assist the communication with the UEs, e.g., imagine the common scenario where both the BS and RIS are deployed at high altitude and their locations are fixed, as shown in Fig. 1. The RIS can dynamically adjust the phase shift induced by each reflecting element on the impinging electromagnetic waves through a perfect smart controller that is connected to the BS in terms of a perfect backhaul link. The size of each RIS element is $d_H \times d_V$, where d_V and d_H express its vertical height and its horizontal width, respectively. The proposed model considers also the potential presence of direct links between the BS and the UEs. However, these could be also neglected in the cases of high penetration losses and/or big signal blockages.

A. Channel Model

We account for a quasi-static fading model with coherence bandwidth much larger than the channel bandwidth. We employ the standard block fading model with each coherence interval/block including $\tau_c = B_c T_c$ channel uses, where B_c and T_c are the coherence bandwidth and the coherence time in Hz and s, respectively.

Within the transmission in each coherence block and during the n th time slot, let $\mathbf{H}_1 = [\mathbf{h}_{11} \dots, \mathbf{h}_{1L}] \in \mathbb{C}^{M \times L}$ and $\mathbf{h}_{2k,n} \in \mathbb{C}^{L \times 1}$ be the LoS channel between the BS and the RIS and the channel between the RIS and UE k at the n th time instant. Note that \mathbf{h}_{1i} for $i = 1, \dots, L$ denotes the i th column vector of \mathbf{H}_1 . Similarly, let $\mathbf{g}_{k,n} \in \mathbb{C}^{M \times 1}$ be the direct channel between the BS and UE k at the n th time instant. Despite that the majority of existing works, e.g., [3], [4], assumed independent Rayleigh model, in practice, correlated fading appears, which affects the performance [30]. Thus, $\mathbf{h}_{2k,n}$ and

$\mathbf{g}_{k,n}$ are described in terms of correlated Rayleigh fading distributions as

$$\mathbf{h}_{2k,n} = \sqrt{\beta_{h_2,k}} \mathbf{R}_{\text{RIS},k}^{1/2} \mathbf{q}_{2k,n}, \quad (1)$$

$$\mathbf{g}_{k,n} = \sqrt{\beta_{g,k}} \mathbf{R}_{\text{BS},k}^{1/2} \mathbf{q}_{k,n}, \quad (2)$$

where $\mathbf{R}_{\text{RIS},k} \in \mathbb{C}^{L \times L}$ and $\mathbf{R}_{\text{BS},k} \in \mathbb{C}^{M \times M}$ express the deterministic Hermitian-symmetric positive semi-definite correlation matrices at the RIS and the BS respectively with $\text{tr}(\mathbf{R}_{\text{RIS},k}) = L$ and $\text{tr}(\mathbf{R}_{\text{BS},k}) = M$. The correlation matrices $\mathbf{R}_{\text{RIS},k}$ and $\mathbf{R}_{\text{BS},k} \forall k$ are assumed to be known by the network since they can be obtained by existing estimation methods [31].² Another way of practical calculation of the covariance matrices follows. Especially, as can be seen by the expression of the covariance matrices, they depend on the distances d_{BS} and d_{IRS} and the angles. The distances are based on the construction of the BS and the IRS. Moreover, the angles can be calculated when the locations are given. Moreover, $\beta_{h_2,k}$ and $\beta_{g,k}$ describe the path-losses of the RIS-UE k and BS-UE k links, respectively. Especially, $\beta_{g,k}$ is expected to be small because of the blockages between the BS and the UEs. Also, $\mathbf{q}_{2k,n} \sim \mathcal{CN}(\mathbf{0}, \mathbf{I}_L)$ and $\mathbf{q}_{k,n} \sim \mathcal{CN}(\mathbf{0}, \mathbf{I}_M)$ denote the corresponding fast-fading vectors at the n th time instant. Note that fast fading vectors change within each coherence block, while the correlation matrices are assumed constant for a large number of coherence blocks.

The high rank LoS channel \mathbf{H}_1 is described as

$$[\mathbf{H}_1]_{m,l} = \sqrt{\beta_1} \exp\left(j \frac{2\pi}{\lambda} (m-1) d_{\text{BS}} \sin \theta_{1,l} \sin \phi_{1,l} + (l-1) d_{\text{RIS}} \sin \theta_{2,m} \sin \phi_{2,m}\right), \quad (3)$$

where β_1 is the path-loss between the BS and RIS, λ is the carrier wavelength, while d_{BS} and d_{RIS} are the inter-antenna separation at the BS and inter-element separation at the RIS, respectively [16]. Also, $\theta_{1,l}$ and $\phi_{1,l}$ denote the elevation and azimuth LoS angles of departure (AoD) at the BS with respect to RIS element l , and $\theta_{2,l}$ and $\phi_{2,l}$ denote the elevation and azimuth LoS angles of arrival (AoA) at the RIS. It is worthwhile to mention that \mathbf{H}_1 can be obtained similarly to the covariance matrices since the dependence of their expressions on the distances and the angles is similar.

The response of the L elements is described by the diagonal RBM $\Theta = \text{diag}(\mu_1 e^{j\theta_1}, \dots, \mu_L e^{j\theta_L}) \in \mathbb{C}^{L \times L}$, where $\theta_l \in [0, 2\pi]$ and $\mu_l \in [0, 1]$ are the phase and amplitude coefficient for RIS element l , respectively. Herein, we assume maximum signal reflection, i.e., $\mu_l = 1 \forall l$ [3].³ For the sake of exposition, the overall channel vector $\mathbf{h}_{k,n} = \mathbf{g}_{k,n} + \mathbf{H}_1 \Theta \mathbf{h}_{2k,n}$, conditioned on Θ is distributed as $\mathbf{h}_{k,n} \sim \mathcal{CN}(\mathbf{0}, \mathbf{R}_k)$, where $\mathbf{R}_k = \beta_{g,k} \mathbf{R}_{\text{BS},k} + \beta_{h_2,k} \mathbf{H}_1 \Theta \mathbf{R}_{\text{RIS},k} \Theta^H \mathbf{H}_1^H$. Given that \mathbf{R}_k

²The correlation matrices and the path-losses are independent of n because these represent effects that vary with time in a much slower pace than the coherence time.

³Recently, it was shown that the amplitude and phase responses are intertwined in practice, while the assumption of independence between the amplitude and the phase shift or even a unity amplitude is unrealistic, e.g., see [32]. However, this assumption regarding independence still allows revealing fundamental properties of the channel aging of the proposed model, while the consideration of the phase shift model in [32] is an interesting idea for extension of the current work, i.e., to study the impact of channel aging on RIS-assisted systems by accounting for this intertwining.

depends on the path-losses, the correlation matrices, and \mathbf{H}_1 , which are all assumed to be known as explained previously, \mathbf{R}_k can also be assumed known by the network.

Remark 1: Although, it is uncommon to meet independent Rayleigh fading in practice [30], in such a case, we have $\mathbf{R}_{\text{RIS},k} = \mathbf{I}_L$. Then, the overall covariance becomes $\mathbf{R}_k = \beta_{d,k} \mathbf{R}_{\text{BS},k} + \beta_{2,k} \mathbf{H}_1 \mathbf{H}_1^H$. Obviously, \mathbf{R}_k does not depend on the RBM and cannot be optimized. Hence, the RIS cannot be exploited. Nevertheless, note that even under these conditions, the RIS enhances the communication with an additional signal to the receiver.

B. Channel Aging

In practice, the relative movement between the UEs and the RIS, i.e., the UE mobility causes a phenomenon, known as channel aging [19]–[21].⁴ In particular, this movement results in a Doppler shift that makes the channel change with time. Hence, contrary to the conventional block fading channel model, the channel coefficients, exhibiting flat fading, vary from symbol to symbol. However, they are constant within one symbol. The symbol duration is assumed smaller than or equal to the coherence time of all UEs. This assumption is common in works studying the impact of channel aging such as [19]–[22]. The channel use is denoted by $n \in \{1, \dots, \tau_c\}$.

Mathematically, the channel realization $\mathbf{h}_{k,n}$ at the n th time instant is modeled as a function of its initial state $\mathbf{h}_{k,0}$ and an innovation component as [22]

$$\mathbf{h}_{k,n} = \alpha_{k,n} \mathbf{h}_{k,0} + \bar{\alpha}_{k,n} \mathbf{e}_{k,n}, \quad (4)$$

where $\mathbf{e}_{k,n} \sim \mathcal{CN}(\mathbf{0}, \mathbf{R}_k)$ denotes the independent innovation component at the n th time instant and $\alpha_{k,n} = J_0(2\pi f_D T_s n)$ is the temporal correlation coefficient of UE k between the channel realizations at time 0 and n with $J_0(\cdot)$ being the zeroth-order Bessel function of the first kind, T_s being the channel sampling duration, and $f_D = \frac{v f_c}{c}$ being the maximum Doppler shift.⁵ Also, we denote $\bar{\alpha}_{k,n} = \sqrt{1 - \alpha_{k,n}^2}$. Note that v is the velocity of the UE, $c = 3 \times 10^8$ m/s is the speed of light, and f_c is the carrier frequency. As can be seen, a higher UE velocity of the UE or higher delay result in decrease of $\alpha_{k,n}$ though not monotonically, since there are some ripples. It is worthwhile to mention that the model in (4) is not autoregressive of first-order as in previous works [19], [20] since the current channel is not determined in terms of its state at the previous time instant, but it depends on its state at an initial time $\mathbf{h}_{k,0}$. The advantage is that the statistics of the model exactly match with that of the Jakes' model [22].

III. CHANNEL ESTIMATION WITH CHANNEL AGING

Perfect CSI is not available in practice but the BS needs to estimate the channel. On this ground, we consider the

⁴Normally, all RIS elements have the same relative movement comparing to a specific UE.

⁵The second-order statistics of the channel including the path-losses and $\alpha_{k,n}$ are estimated during the connection establishment when the BS estimates the location and the velocity of the UE. While the path-losses are estimated using the average pilot power, $\alpha_{k,n}$ can be estimated using the temporal correlation among the same set of pilots.

standard time-division-duplex (TDD) protocol, where each block consists of τ channel uses for the uplink training phase and $\tau_d = \tau_c - \tau$ channel uses for the downlink data transmission phase [33]. The disadvantage of RIS-assisted systems is that the RIS, which consists of passive elements, cannot process the received pilot symbols from the UEs to obtain the estimated channels and cannot send pilots to the BS for CE. Herein, contrary to ON/OFF channel estimation schemes such as [14] and [16] that require $L + 1$ phases, we perform the CE in a single phase. Notably, the consideration of the cascaded channel CE instead of the individual channels has already been applied in several works such as [5], [6]. Actually, it is more beneficial to consider the overall channel because this allows computing the correlation among inter-element links, while in the case of individual channels, this correlation remains unknown. Also, our CE is accompanied by reduced feedback and allows higher achievable SE due to the larger pre-log factor since the training overhead is much lower.

During the uplink training phase, each UE transmits a τ -length mutually orthogonal training sequences, i.e., $\psi_k = [\psi_{k,1}, \dots, \psi_{k,\tau}]^T \in \mathbb{C}^{\tau \times 1}$. We assume that the pilot sequence consists of K pilot symbols, which is the minimal number for channel estimation, i.e., $\tau \geq K$ [34]. Also, Θ is assumed fixed. Thus, the received signal by the BS at time n is given by

$$\mathbf{Y}_n = \sqrt{p_p} \sum_{i=1}^K \mathbf{h}_{i,n} \psi_i^H + \mathbf{W}_n, \quad (5)$$

where $p_p \geq 0$ is the common pilot transmit power for all UEs and $\mathbf{W}_n \in \mathbb{C}^{M \times \tau}$ is spatially white additive Gaussian noise matrix at the BS during this phase. After correlation of the received signal with the training sequence of UE k $\frac{1}{\sqrt{p_p}} \psi_k$, we obtain

$$\tilde{\mathbf{y}}_{k,n} = \mathbf{h}_{k,n} + \frac{1}{\sqrt{p_p}} \tilde{\mathbf{w}}_{k,n}, \quad (6)$$

where $\tilde{\mathbf{w}}_{k,n} = \mathbf{W}_n \psi_k \sim \mathcal{CN}(\mathbf{0}, \tilde{\sigma}^2 \mathbf{I}_M)$.

Although this received signal can be used to estimate the channel at any time slot of the block, the estimated channel will deteriorate as the time interval between training and transmission increases. On this ground, we consider the channel estimate at $n = K + 1$ since the estimate will be worse at a later instant. Based on (4), the channel at the n th instant ($n \leq K$) can be described in terms of the channel at time $K + 1$ as

$$\mathbf{h}_{k,n} = \alpha_{k,\zeta-n} \mathbf{h}_{k,\zeta} + \bar{\alpha}_{k,\zeta-n} \tilde{\mathbf{e}}_{k,n}, \quad (7)$$

where $\tilde{\mathbf{e}}_{k,n} \sim \mathcal{CN}(\mathbf{0}, \mathbf{R}_k)$ is the independent innovation vector, which relates $\mathbf{h}_{k,n}$ and $\mathbf{h}_{k,\zeta}$. Also, we have defined $\zeta = K + 1$ to simplify the notation. Inserting (7) into (6), we obtain

$$\tilde{\mathbf{y}}_{k,n} = \alpha_{k,\zeta-n} \mathbf{h}_{k,\zeta} + \bar{\alpha}_{k,\zeta-n} \tilde{\mathbf{e}}_{k,n} + \frac{1}{\sqrt{p_p}} \tilde{\mathbf{w}}_{k,n}. \quad (8)$$

By applying the standard minimum mean square error (MMSE) estimation [33], the BS obtains the channel estimate

of $\mathbf{h}_{k,\zeta}$ as

$$\hat{\mathbf{h}}_{k,\zeta} = \alpha_{k,\zeta-n} \mathbf{R}_k \mathbf{Q} \tilde{\mathbf{y}}_{k,n}, \quad (9)$$

where $\mathbf{Q} = \left(\mathbf{R}_k + \frac{\tilde{\sigma}^2}{p_p} \mathbf{I}_M \right)^{-1}$. The estimate $\hat{\mathbf{h}}_{k,\zeta}$ is distributed as $\mathcal{CN}(\mathbf{0}, \Phi_k)$, where $\Phi_k = \alpha_{k,\zeta-n}^2 \mathbf{R}_k \mathbf{Q} \mathbf{R}_k$. According to the orthogonality property of MMSE estimation, the independent channel estimation error vector is $\tilde{\mathbf{h}}_{k,\zeta} = \mathbf{h}_{k,\zeta} - \hat{\mathbf{h}}_{k,\zeta}$ and distributed as $\mathcal{CN}(\mathbf{0}, \Psi_k)$, where $\Psi_k = \mathbf{R}_k - \Phi_k$. Notably, the channel estimate $\hat{\mathbf{h}}_{k,\zeta}$ in (9) includes the degradation due to the channel aging.

Remark 2: In the case of no channel aging, i.e., when $\alpha_{k,\zeta-n} = 1$, we reduce to the conventional block-fading model. Moreover, as can be seen, the estimation error takes values between $\mathbf{R}_k (\mathbf{I}_M - \alpha_{k,1}^2 \mathbf{Q} \mathbf{R}_k)$ and $\mathbf{R}_k (\mathbf{I}_M - \alpha_{k,K}^2 \mathbf{Q} \mathbf{R}_k)$. Also, we observe that in the case of no mobility, the estimation error vanishes as the pilot signal-to-noise ratio (SNR) $\gamma = \frac{p_p}{\tilde{\sigma}^2}$ increases, while it saturates as $\lim_{\gamma \rightarrow \infty} \Psi_k = (1 - \alpha_{k,\zeta-n}^2) \mathbf{R}_k$ in the case of channel aging. The latter shows that the estimation error increases as the UE moves with higher velocity and as the number of UEs increases since ζ increases.

In Sec. VI, we illustrate the normalized mean square error (NMSE) defined as

$$\text{NMSE}_k = \frac{\text{tr}(\mathbb{E}[(\hat{\mathbf{h}}_k - \mathbf{h}_k)(\hat{\mathbf{h}}_k - \mathbf{h}_k)^H])}{\text{tr}(\mathbb{E}[\mathbf{h}_k \mathbf{h}_k^H])} \quad (10)$$

$$= 1 - \frac{\text{tr}(\Psi_k)}{\text{tr}(\mathbf{R}_k)}. \quad (11)$$

According to (11), an increase in channel aging results in the increase of the NMSE_k . Overall, channel aging has a detrimental on channel estimation. Below, we elaborate on its impact during the downlink transmission.

IV. DOWNLINK TRANSMISSION

The downlink transmission of data from the BS to all UEs consists of a broadcast channel that has to make use of a certain precoding strategy in terms of a precoding vector $\mathbf{f}_{k,n} \in \mathbb{C}^{M \times 1}$. In parallel, taking advantage of TDD and its channel reciprocity, the downlink channel is the Hermitian transpose of the uplink channel. Thus, the received signal $r_{k,n} \in \mathbb{C}$ by UE k during the data transmission phase ($n = K + 1, \dots, \tau_c$) can be written as

$$r_{k,n} = \mathbf{h}_{k,n}^H \mathbf{s}_n + z_{k,n}, \quad (12)$$

where $\mathbf{s}_n = \sum_{i=1}^K \sqrt{p_i} \mathbf{f}_{i,n} x_{i,n}$ describes the transmit signal vector by the BS, $p_i \geq 0$ is the transmit power to UE i , and $z_{k,n} \sim \mathcal{CN}(0, \sigma^2)$ is complex Gaussian noise at UE k . Note that $\mathbf{f}_{i,n} \in \mathbb{C}^{M \times K}$ and $x_{i,n}$ are the linear precoding vector and the data symbol with $\mathbb{E}\{|x_{i,n}|^2\} = 1$, respectively.⁶ The precoding vector is normalized based on the average total power constraint

$$\mathbb{E}\{\|\mathbf{s}_n\|^2\} = \text{tr}(\mathbf{P} \mathbf{F}_n^H \mathbf{F}_n) \leq P_{\max}, \quad (13)$$

⁶If we assume that mmWave communication takes place, hybrid beamforming can be introduced as the best solution that achieves a good trade-off between cost and complexity as usually adopted in the literature. However, the study of the impact of channel aging in the mmWave region is left for future research due to limited space.

where $\mathbf{F}_n = [\mathbf{f}_{1,n}, \dots, \mathbf{f}_{K,n}] \in \mathbb{C}^{M \times K}$, $\mathbf{P} = \text{diag}(p_1, \dots, p_K)$, and $P_{\max} > 0$ is the total transmit power. However, the channel $\mathbf{h}_{k,n}$ in (12) can be expressed as

$$\begin{aligned} \mathbf{h}_{k,n} &= \alpha_{k,n-K} \hat{\mathbf{h}}_k + \alpha_{k,n-K} \tilde{\mathbf{h}}_k + \bar{\alpha}_{k,n-K} \tilde{\mathbf{e}}_{k,n} \\ &\quad \alpha_{k,n-K} \hat{\mathbf{h}}_k + \bar{\alpha}_{k,n-K} \tilde{\mathbf{e}}_{k,n}, \end{aligned} \quad (14)$$

where $\hat{\mathbf{h}}_k$ expresses the channel vector at the beginning of the data transmission phase, and $\tilde{\mathbf{h}}_k$ is the corresponding channel estimation error.

Substitution of (14) into (12) provides

$$\begin{aligned} r_{k,n} &= \alpha_{k,n-K} \sqrt{p_k} \mathbf{h}_k^H \mathbf{f}_{k,n} x_{k,n} + \bar{\alpha}_{k,n-K} \sqrt{p_k} \tilde{\mathbf{e}}_{k,n}^H \mathbf{f}_{k,n} x_{k,n} \\ &\quad + \sum_{i \neq k}^K \sqrt{p_i} \mathbf{h}_{k,n}^H \mathbf{f}_{i,n} x_{i,n} + z_{k,n}. \end{aligned} \quad (15)$$

Although UEs do not have instantaneous CSI, we can assume that UE k has access to $\mathbb{E}\{\hat{\mathbf{h}}_k^H \mathbf{f}_{k,n} x_{k,n}\}$. Then, by using the technique in [35], where UE k is aware of only the statistical CSI, the received signal is written as

$$\begin{aligned} r_{k,n} &= \alpha_{k,n-K} \sqrt{p_k} \mathbb{E}\{\mathbf{h}_k^H \mathbf{f}_{k,n}\} x_{k,n} + \bar{\alpha}_{k,n-K} \sqrt{p_k} \tilde{\mathbf{e}}_{k,n}^H \mathbf{f}_{k,n} x_{k,n} \\ &\quad + \alpha_{k,n-K} \sqrt{p_k} \mathbf{h}_k^H \mathbf{f}_{k,n} x_{k,n} - \alpha_{k,n-K} \sqrt{p_k} \mathbb{E}\{\mathbf{h}_k^H \mathbf{f}_{k,n}\} x_{k,n} \\ &\quad + \sum_{i \neq k}^K \sqrt{p_i} \mathbf{h}_{k,n}^H \mathbf{f}_{i,n} x_{i,n} + z_{k,n}. \end{aligned} \quad (16)$$

Proposition 1: The downlink average SE for UE k of an RIS-assisted mMIMO system, accounting for imperfect CSI and channel aging, is lower bounded by

$$\text{SE}_k = \frac{1}{\tau_c} \sum_{n=K+1}^{\tau_c} \log_2(1 + \gamma_{k,n}), \quad (17)$$

where $\gamma_{k,n}$ is the achievable SINR at time n given by (18).

Proof: First, based on a similar approach to [36], [37], the average achievable SE including the achievable SINR $\gamma_{k,n}$ in the transmission phase is computed for each n . Next, the average over these SEs is obtained as in (17).

Regarding the achievable SINR $\gamma_{k,n}$, given the Gaussianity of the input symbols, it is obtained by accounting for a worst-case assumption for the computation of the mutual information [34, Theorem 1]. In particular, except for $\mathbb{E}\{\hat{\mathbf{h}}_k^H \mathbf{f}_{k,n}\}$ being the deterministic desired signal detected by UE k , all others terms are treated as independent Gaussian noise with zero mean and variance equal to the variance of interference plus noise. ■

The following analysis requires M , L , and K increase but with a given bounded ratio as $0 < \liminf \frac{K}{M} \leq \limsup \frac{K}{M} < \infty$ and $0 < \liminf \frac{L}{M} \leq \limsup \frac{L}{M} < \infty$. Henceforth, this notation is denoted as $M \rightarrow \infty$. Taking into account that, according to (14), the available CSI at time n is $\alpha_{k,n-K} \hat{\mathbf{h}}_k$,

the BS designs its RZF precoder as⁷

$$\mathbf{f}_{k,n} = \alpha_{k,n-K} \sqrt{\lambda} \Sigma \hat{\mathbf{h}}_k, \quad (19)$$

where λ is a normalization parameter, which is obtained due to (13) as

$$\lambda = \frac{P_{\max}}{\alpha_{k,n-K}^2 \text{tr}(\mathbf{P} \hat{\mathbf{H}}^H \Sigma^2 \hat{\mathbf{H}})}. \quad (20)$$

Note that $\Sigma \triangleq (\alpha_{k,n-K}^2 \hat{\mathbf{H}} \hat{\mathbf{H}}^H + \mathbf{Z} + M \alpha \mathbf{I}_M)^{-1}$, where $\mathbf{Z} \in \mathbb{C}^{M \times M}$ is an arbitrary Hermitian non negative definite matrix, and α is a regularization scaled by M to make expressions converge to a constant as $M \rightarrow \infty$. As a result, by denoting $\rho = \frac{P_{\max}}{\sigma^2}$ the SNR at the downlink transmission phase, the SINR of UE k under RZF precoding can be written as (21) at the top of the next page. For the sake of convenience, we denote $S_{k,n}$ and $I_{k,n}$ the numerator and denominator of (21), respectively, i.e., we have $\gamma_{k,n} = \frac{S_{k,n}}{I_{k,n}}$.

Based on similar assumptions to [38, Assump. A1-A3] regarding the covariance matrices under study, we rely on the DE analysis to obtain the DE downlink SE of UE k .⁸ The DE SINR obeys to $\gamma_{k,n} - \bar{\gamma}_{k,n} \xrightarrow[M \rightarrow \infty]{\text{a.s.}} 0$ while the deterministic SE of UE k obeys to

$$\text{SE}_k - \bar{\text{SE}}_k \xrightarrow[M \rightarrow \infty]{\text{a.s.}} 0, \quad (22)$$

where $\bar{\text{SE}}_k = \frac{1}{\tau_c} \sum_{n=K+1}^{\tau_c} \log_2(1 + \bar{\gamma}_{k,n})$ based on the dominated convergence and the continuous mapping theorem [39].

Theorem 1: The downlink DE of the SINR of UE k with RZF precoding at time n , accounting for correlated Rayleigh fading, imperfect CSI, and channel aging due to UE mobility is given by (23), where

$$\bar{\lambda} = \frac{P_{\max}}{\frac{1}{M} \sum_{i=1}^K p_i \frac{\alpha_{k,n-K}^2 \delta_i^\lambda}{(1 + \alpha_{k,n-K}^2 \delta_i)^2}}, \quad (24)$$

$\delta_k = \frac{1}{M} \text{tr}(\Phi_k \mathbf{T})$, $\tilde{\delta}_k = \frac{1}{M^2} \text{tr}((\mathbf{R}_k - \Phi_k) \tilde{\mathbf{T}}(\Phi_k))$, $\delta_k^e = \frac{1}{M} \text{tr}(\mathbf{R}_k \tilde{\mathbf{T}}(\Phi_k))$, $\delta_i^\lambda = \frac{1}{M} \text{tr}(\Phi_i \tilde{\mathbf{T}}(\mathbf{I}_M))$, $\zeta_{ki} = \frac{1}{M^2} \text{tr}(\mathbf{R}_k \tilde{\mathbf{T}}(\Phi_i))$, $\mu_{ki} = \frac{1}{M^2} \text{tr}(\Phi_k \tilde{\mathbf{T}}(\Phi_i))$, $Q_{ik} = \zeta_{ki} + \frac{|\delta_k|^2 \mu_{ki}}{(1 + \alpha_{k,n-K}^2 \delta_k)^2} - 2 \text{Re} \left\{ \frac{\delta_k^* \mu_{ki}}{1 + \alpha_{k,n-K}^2 \delta_k} \right\}$, with

$$\begin{aligned} * \mathbf{T} &= \left(\sum_{i=1}^K \frac{1}{M (1 + \alpha_{i,n-K}^2 \delta_i)} \Phi_i + \alpha \mathbf{I}_M \right)^{-1}, \\ * \tilde{\mathbf{T}}(\mathbf{L}) &= \mathbf{T} \mathbf{L} \Phi_i \mathbf{T} + \sum_{i=1}^K \frac{\tilde{\delta}_i \mathbf{T} \Phi_i \mathbf{T}}{M (1 + \alpha_{i,n-K}^2 \delta_i)^2}, \mathbf{L} = \Phi_i, \mathbf{I}_M \end{aligned}$$

⁷Despite that RZF precoding is generally suboptimal, it has been applied selected in the case of mMIMO in many works due to reasons of complexity and to provide closed-form expressions. In other words, it is common in mMIMO to consider a linear precoder between the MRT and RZF precoders. Hence, for these reasons, in this work, we have selected the more optimal precoder, i.e., RZF despite its complexity. Note that RZF precoding is a very good choice compared to MRT, and the corresponding derivation of the rate together with its optimization require delicate manipulations, which raise the novelty of this work.

⁸The DE analysis results in deterministic expressions, which make lengthy Monte-Carlo simulations unnecessary. Also, its results are tight approximations even for conventional systems with moderate dimensions, e.g., an 8×8 matrix [39]. Hence, the following DE SINR in (23) is of great practical importance.

$$\gamma_{k,n} = \frac{\alpha_{k,n-K}^2 p_k |\mathbb{E}\{\mathbf{h}_k^H \mathbf{f}_{k,n}\}|^2}{\alpha_{k,n-K}^2 p_k \text{Var}\{\mathbf{h}_k^H \mathbf{f}_{k,n}\} + \sum_{i \neq k}^K \alpha_{i,n-K} p_i \mathbb{E}\{|\mathbf{h}_{k,n}^H \mathbf{f}_{i,n}|^2\} + \bar{\alpha}_{k,n-K}^2 p_k \mathbb{E}\{|\tilde{\mathbf{e}}_{k,n}^H \mathbf{f}_{k,n}|^2\} + \sigma^2}. \quad (18)$$

$$\gamma_{k,n} = \frac{p_k |\mathbb{E}\{\mathbf{h}_k^H \Sigma \hat{\mathbf{h}}_k\}|^2}{p_k \text{Var}\{\mathbf{h}_k^H \Sigma \hat{\mathbf{h}}_k\} + \sum_{i \neq k}^K p_i \frac{\alpha_{i,n-K}^4}{\alpha_{k,n-K}^4} \mathbb{E}\{|\mathbf{h}_{k,n}^H \Sigma \hat{\mathbf{h}}_i|^2\} + p_k \frac{\bar{\alpha}_{k,n-K}^2}{\alpha_{k,n-K}^2} \mathbb{E}\{|\tilde{\mathbf{e}}_{k,n}^H \Sigma \hat{\mathbf{h}}_k|^2\} + \frac{\text{tr}(\mathbf{P} \hat{\mathbf{H}}^H \Sigma^2 \hat{\mathbf{H}})}{\alpha_{k,n-K}^2}}. \quad (21)$$

$$\tilde{\gamma}_{k,n} = \frac{p_k \delta_k^2}{p_k \tilde{\delta}_k + p_k \frac{\bar{\alpha}_{k,n-K}^2}{\alpha_{k,n-K}^2} \delta_k^e + \sum_{i \neq k}^K p_i \frac{\alpha_{i,n-K}^4 (1 + \alpha_{k,n-K}^2 \delta_k)^2}{\alpha_{k,n-K}^4 (1 + \alpha_{i,n-K}^2 \delta_i)^2} Q_{ik} + \frac{1}{M} \sum_{i=1}^K p_i \frac{(1 + \alpha_{k,n-K}^2 \delta_k)^2 \delta_i^\lambda}{\rho (1 + \alpha_{i,n-K}^2 \delta_i)^2}}. \quad (23)$$

$$* \tilde{\delta}(\mathbf{L}) = \frac{1}{M^2 (1 + \alpha_{i,n-K}^2 \delta_i)} \text{tr}(\mathbf{\Phi}_k \mathbf{T} \mathbf{L} \mathbf{T}), \quad \mathbf{L} = \mathbf{\Phi}_i, \mathbf{I}_M.$$

Proof: : Please see Appendix A. ■

convergence to the optimum value since the sum rate is upper-bounded subject to the power constraint (25c). Note that all computations take place at the BS.

V. SUM SE MAXIMIZATION

In this section, we focus on the optimization of the sum SE of a RIS-assisted time-varying mMIMO system with channel aging. Specifically, the sum rate maximization problem is described as

$$(\mathcal{P}1) \quad \max_{\Theta, \mathbf{p} \geq 0} \overline{\text{SE}} = \sum_{i=1}^K \overline{\text{SE}}_i \quad (25a)$$

$$\text{s.t.} \quad |\tilde{\theta}_l| = 1, \quad l = 1, \dots, L, \quad (25b)$$

$$\sum_{i=1}^K p_i \leq P_{\max}, \quad (25c)$$

where we have denoted the elements of Θ as $\tilde{\theta}_l = \exp(j\theta_l)$ for all l and the vector $\mathbf{p} = [p_1, \dots, p_K]^T$. The first constraint in (25b) means that each RIS element induces a phase shift without any change on the amplitude of the incoming signal, while constraint (25c) ensures that the BS transmit power is kept below the maximum power P_{\max} .⁹

The solution of the optimization problem (P1) is challenging due to its non-convexity and the unit-modulus constraint concerning $\tilde{\theta}_l$. To tackle this difficulty, we consider the alternating optimization (AO) technique, where Θ and \mathbf{p} are going to be solved separately and iteratively. In particular, first, we focus on finding the optimum Θ given fixed \mathbf{p} . Next, we solve for \mathbf{p} with fixed Θ . The iteration of this procedure, where the sum rate increases at each iteration step, continues until

⁹The considered optimization problem allocates the available resources (power vector, RIS configuration) to maximize the total spectral efficiency (i.e., sum-rate). This is a well-known objective function when the total/aggregate rate of the network is the key design priority. It is worth also noting that the sum capacity/rate is a fundamental performance metric (one dimension) in multi-user networks from information theoretic perspective. To consider QoS per individual user, the consideration of other objective functions that take into account fairness (e.g. max-min rate) and/or minimum individual rates is required, which are beyond the scope of this paper and can be considered for future work.

A. RIS Configuration

The exploitation of the RIS potentials implies the optimization of the RBM towards maximum sum SE. The presence of the RBM appears inside the covariance matrices in the DE achievable SINR in (23). Given that the logarithm function is monotonic, it is sufficient to maximize $\tilde{\gamma}_{k,n}$ instead of $\overline{\text{SE}}_k$. Hence, by assuming infinite resolution phase shifters, the RBM optimization problem is formulated as

$$(\mathcal{P}2) \quad \max_{\Theta} \overline{\text{SE}} \quad (26)$$

$$\text{s.t.} \quad |\tilde{\theta}_l| = 1, \quad l = 1, \dots, L.$$

Although the problem (P2) is non-convex in terms of Θ and it is subject to a unit-modulus constraint regarding $\tilde{\theta}_l$, application of the projected gradient ascent algorithm can achieve a local optimal solution by projecting the solution onto the closest feasible point at every step until converging to a stationary point. Specifically, let the vector $\mathbf{c}_t = [\tilde{\theta}_{t,1}, \dots, \tilde{\theta}_{t,L}]^T$ include the phases at step t . The next step of the algorithm is described by

$$\tilde{\mathbf{c}}_{t+1} = \mathbf{c}_t + \tilde{\mu} \mathbf{q}_t, \quad \mathbf{c}_{t+1} = \exp(j \arg(\tilde{\mathbf{c}}_{t+1})), \quad (27)$$

where the parameter $\tilde{\mu}$ denotes the step size and $\mathbf{q}_t = \frac{\partial \tilde{\gamma}_{k,n}}{\partial \mathbf{c}_t}$ describes the ascent direction at step t , given below by Proposition 2.¹⁰ Note that the suitable step size at each iteration is selected based on the backtracking line search [40]. The solution is obtained by the projection problem $\min_{|\theta_l|=1, l=1, \dots, L} \|\mathbf{c} - \tilde{\mathbf{c}}\|^2$ under the unit-modulus constraint. Algorithm 1 presents the overview of this procedure. For the sake of convenience, we denote the partial derivative with respect to \mathbf{c}_t^* by $(\cdot)'$.

¹⁰Given that the feasible set is the unit circle, then any point x should be projected on this circle, i.e., it should be $x/|x|$, which is equal to $\exp(j\angle(x))$.

Algorithm 1 Projected Gradient Ascent Algorithm for the RIS Design

1. **Initialisation:** $\mathbf{c}_0 = \exp(j\pi/2) \mathbf{1}_L$, $\Theta_0 = \text{diag}(\mathbf{c}_0)$, $\bar{\gamma}_{k,n} = f(\Theta_0)$ given by (23); $\epsilon > 0$
 2. **Iteration t :** for $t = 0, 1, \dots$, do
 3. $\mathbf{q}_t = \frac{\partial \bar{\gamma}_{k,n}}{\partial \mathbf{c}_t^*}$, where $\frac{\partial \bar{\gamma}_{k,n}}{\partial \mathbf{c}_t^*}$ is given by Proposition 2;
 4. **Find** $\bar{\mu}$ by backtrack line search ($f(\Theta_0)$, $\mathbf{q}_t, \mathbf{c}_t$) [40];
 5. $\tilde{\mathbf{c}}_{t+1} = \mathbf{c}_t + \bar{\mu} \mathbf{q}_t$;
 6. $\mathbf{c}_{t+1} = \exp(j \arg(\tilde{\mathbf{c}}_{t+1}))$; $\Theta_{t+1} = \text{diag}(\mathbf{c}_{t+1})$;
 7. $\bar{\gamma}_{k,n}^{t+1} = f(\Theta_{t+1})$;
 8. **Until** $\|\bar{\gamma}_{k,n}^{t+1} - \bar{\gamma}_{k,n}^t\| < \epsilon$; **Obtain** $\Theta^* = \Theta_{t+1}$;
 9. **end for**
-

Proposition 2: The derivative of $\bar{\gamma}_{k,n}$ with respect to \mathbf{c}_t^* is given by

$$\bar{\gamma}'_{k,n} = \frac{S'_k I_k - S_k I'_k}{I_k^2}, \quad (28)$$

where

$$\begin{aligned} S'_k &= 2p_k \delta_k \delta'_k, \\ I'_k &= \tilde{\delta}'_k + (\delta_k^e)' + \sum_{i \neq k} \frac{\alpha_{i,n-K}^2 (1 + \alpha_{k,n-K}^2 \delta_k)^2}{\alpha_{k,n-K}^2 (1 + \alpha_{i,n-K}^2 \delta_i)^2} Q'_{ik} \\ &+ \frac{1}{M} \sum_{i=1}^K p_i \frac{2(1 + \alpha_{k,n-K}^2 \delta_k) \delta_k' \delta_i^\lambda + (1 + \alpha_{k,n-K}^2 \delta_k)^2 (\delta_i^\lambda)'}{(1 + \alpha_{i,n-K}^2 \delta_i)^2} \\ &+ \frac{1}{M} \sum_{i=1}^K p_i \frac{\alpha_{i,n-K}^2 (1 + \alpha_{k,n-K}^2 \delta_k)^2 \rho \delta_i' \delta_i^\lambda}{(1 + \alpha_{i,n-K}^2 \delta_i)^3} \\ &+ \sum_{i \neq k} \frac{2\alpha_{i,n-K}^2 \alpha_{k,n-K}^2 \delta_k' (1 + \alpha_{k,n-K}^2 \delta_k)}{\alpha_{k,n-K}^2 \rho (1 + \alpha_{i,n-K}^2 \delta_i)^3} Q_{ik} \\ &- \sum_{i \neq k} \frac{3\alpha_{i,n-K}^4 \delta_i' (1 + \alpha_{k,n-K}^2 \delta_k)^2}{\alpha_{k,n-K}^2 (1 + \alpha_{i,n-K}^2 \delta_i)^5} Q_{ik} \end{aligned} \quad (30)$$

with the auxiliary variables given by

$$\tilde{\delta}'_k = \frac{1}{M} \text{tr}((\mathbf{R}'_k - \Phi'_k) \tilde{\mathbf{T}}(\Phi_k) + (\mathbf{R}_k - \Phi_k) \tilde{\mathbf{T}}'(\Phi_k)), \quad (31)$$

$$(\delta_k^e)' = \frac{1}{M} \text{tr}(\mathbf{R}'_k \tilde{\mathbf{T}}(\Phi_k) + \mathbf{R}_k \tilde{\mathbf{T}}'(\Phi_k)), \quad (32)$$

$$\mathbf{T}' = -\mathbf{T}(\mathbf{T}^{-1})' \mathbf{T}, \quad (33)$$

$$(\mathbf{T}^{-1})' = \frac{1}{M} \sum_{i=1}^K \frac{\Phi'_i (1 + \alpha_{i,n-K}^2 \delta_i) - \alpha_{i,n-K}^2 \Phi_i \delta_i'}{(1 + \alpha_{i,n-K}^2 \delta_i)^2}, \quad (34)$$

$$\begin{aligned} \tilde{\mathbf{T}}'(\Phi_k) &= \mathbf{T}' \Phi_k \mathbf{T} + \mathbf{T} \Phi_k' \mathbf{T} + \mathbf{T} \Phi_k \mathbf{T}' \\ &+ \frac{1}{M} \sum_{i=1}^K \frac{\tilde{\delta}'_i \mathbf{T} \Phi_i \mathbf{T} + \tilde{\delta}_i (\mathbf{T}' \Phi_k \mathbf{T} + \mathbf{T} \Phi_k' \mathbf{T} + \mathbf{T} \Phi_k \mathbf{T}')}{(1 + \alpha_{i,n-K}^2 \delta_i)^3} \\ &- \frac{1}{M} \sum_{i=1}^K \frac{2\alpha_{i,n-K}^2 \tilde{\delta}_i \mathbf{T} \Phi_i \mathbf{T} \delta_i'}{(1 + \alpha_{i,n-K}^2 \delta_i)}, \end{aligned} \quad (35)$$

$$\begin{aligned} Q'_{ik} &= \zeta'_{ki} + \frac{\delta_k \delta'_k \mu_{ki} + |\delta_k|^2 \mu_{ki}}{(1 + \alpha_{k,n-K}^2 \delta_k)^2} + \frac{2\alpha_{k,n-K}^2 |\delta_k|^2 \mu_{ki} \delta'_k}{(1 + \alpha_{k,n-K}^2 \delta_k)^3} \\ &- 2\text{Re} \left\{ \frac{(\delta_k^e)' \mu_{ki} + \delta_k^* \mu'_{ki}}{1 + \alpha_{k,n-K}^2 \delta_k} + \frac{\alpha_{k,n-K}^2 \delta_k^* \mu_{ki} \delta'_k}{(1 + \alpha_{k,n-K}^2 \delta_k)^2} \right\}, \end{aligned} \quad (36)$$

$$\zeta'_{ki} = \frac{1}{M^2} \text{tr}(\mathbf{R}'_k \tilde{\mathbf{T}}(\Phi_i) + \mathbf{R}_k \tilde{\mathbf{T}}'(\Phi_i)), \quad (37)$$

$$\mu'_{ki} = \frac{1}{M^2} \text{tr}(\Phi'_k \tilde{\mathbf{T}}(\Phi_i) + \Phi_k \tilde{\mathbf{T}}'(\Phi_i)), \quad (38)$$

$$\bar{\lambda}' = \frac{K \left(\frac{1}{M} \text{tr} \left(\frac{\mathbf{Z}}{M} + \alpha \mathbf{I}_M \right) \tilde{\mathbf{T}}'(\mathbf{I}_M) - \frac{1}{M} \text{tr} \mathbf{T}' \right)}{\left(\frac{1}{M} \text{tr} \mathbf{T} - \frac{1}{M} \text{tr} \left(\frac{\mathbf{Z}}{M} + \alpha \mathbf{I}_M \right) \tilde{\mathbf{T}}(\mathbf{I}_M) \right)^2}. \quad (39)$$

Proof: The proof is given in Appendix B. \blacksquare

The RBM beamforming design is based on the gradient ascent, which results in a significant advantage because the gradient ascent is derived in a closed-form. This method comes with low computational complexity because it consists of simple matrix operations. Specifically, the complexity of Algorithm 1 is $\mathcal{O}(MN^2 + N + M)$, which consists of the fundamental system parameters M and N with the number of RIS elements having the higher (square) impact.

B. Power Allocation

Given a fixed RBM Θ , the objective is the maximization of the sum SE with respect to \mathbf{p} . Specifically, we have

$$\begin{aligned} (\mathcal{P}3) \quad & \max_{\mathbf{p} \geq 0} \quad \overline{\text{SE}} \\ & \text{s.t.} \quad \sum_{i=1}^K p_i \leq P_{\max}, \end{aligned} \quad (40)$$

where $\overline{\text{SE}}$ is given by (25a). This problem is not convex but a local optimal solution can be obtained by using a weighted minimum mean square error (MMSE) reformulation of the sum SE maximization. The SINR $\bar{\gamma}_{k,n}$ in (23) can be described as a function of the downlink power coefficients given by the vector \mathbf{p} as

$$\bar{\gamma}_{k,n} = \frac{p_k q_k}{\mathbf{c}^\top \mathbf{p}}, \quad (41)$$

where $\mathbf{c} = [c_1, \dots, c_K]^\top$ with

$$q_k = \delta_k^2, \quad (42)$$

$$c_k = \tilde{\delta}_k + \frac{\bar{\alpha}_{k,n-K}^2}{\alpha_{k,n-K}^2} \delta_k^e + \frac{1}{M} \delta_i^\lambda, \quad \forall g \quad (43)$$

$$\begin{aligned} c_{gi} &= \frac{\alpha_{i,n-K}^4 (1 + \alpha_{k,n-K}^2 \delta_k)^2}{\alpha_{k,n-K}^4 (1 + \alpha_{i,n-K}^2 \delta_i)^2} Q_{ik} \\ &+ \frac{1}{M} \frac{(1 + \alpha_{k,n-K}^2 \delta_k)^2 \delta_i^\lambda}{(1 + \alpha_{i,n-K}^2 \delta_i)^2}, \quad \forall g, \quad \forall i \neq g. \end{aligned} \quad (44)$$

The MMSE reformulation includes writing the SINR in (41) in terms of a single-input and single-output (SISO) channel that is described as

$$\tilde{y}_k = \sqrt{p_k q_k} s_k + \sum_{i=1}^K \sqrt{p_i c_i} s_i, \quad (45)$$

where \tilde{y}_k is the received signal, and $s_i \in \mathbb{C}$ expresses the normalized and independent random data signal with $\mathbb{E}\{|s_i|^2\} = 1$. The receiver can compute an estimate $\hat{s}_k = v_k^* \tilde{y}_k$ of the desired signal s_k by minimizing the MSE $e_k(\mathbf{p}, v_k) = \mathbb{E}\{|\hat{s}_k - s_k|^2\}$, where v_k as a scalar combining coefficient. Specifically, the MSE is written as

$$e_k(\mathbf{p}, v_k) = v_k^2 (p_k q_k + \mathbf{c}^\top \mathbf{p}) - 2v_k \sqrt{p_k q_k} + 1. \quad (46)$$

The coefficient v_k , which minimizes the MSE $e_k(\mathbf{p}, v_k)$ for a given \mathbf{p} , is given by

$$v_k = \frac{\sqrt{p_k q_k}}{p_k q_k + \sum_{i=1}^K p_i c_i}. \quad (47)$$

Substituting v_k into (46), the MSE becomes $1/(1 + \bar{\gamma}_{k,n})$. According to the weighted MMSE method, we introduce the auxiliary weight parameter $d_k \geq 0$ for the MSE e_k and focus on the solution of the following optimization problem

$$(\mathcal{P4}) \quad \min_{\substack{\mathbf{p} \geq 0, \\ \{v_k, d_k \geq 0: k=1, \dots, K\}}} \sum_{i=1}^K d_i e_i(\mathbf{p}, \mathbf{v}_i) - \ln(d_i) \quad (48)$$

$$\text{s.t.} \quad \sum_{i=1}^K p_i \leq P_{\max}.$$

It is worthwhile to mention that problems $(\mathcal{P3})$ and $(\mathcal{P4})$ are equivalent because they have the same global optimal solution. The equivalence relies on the fact that the optimal d_k in (48) is $1/e_k = (1 + \bar{\gamma}_{k,n})$. The benefit of the reformulation results in the following lemma, which is adapted based on [41, Th. 3].

Lemma 1: The block descent coordinate algorithm, described as Algorithm 2 below, converges to a local optimum of $(\mathcal{P4})$ by means of AO among three blocks of variables being $\{v_k : k = 1, \dots, K\}$, $\{d_k : k = 1, \dots, K\}$, and \mathbf{p} .

Algorithm 2 Block coordinate descent algorithm for solving $(\mathcal{P4})$

1. **Initialisation:** Set $\mathbf{p} = \frac{P_{\max}}{K} \mathbf{1}_K$ (arbitrary value) and the solution accuracy $\epsilon > 0$,
2. **while** the objective function in (48) is not improved more than ϵ **do**
3. $v_k = \frac{\sqrt{p_k q_k}}{p_k q_k + \sum_{i=1}^K p_i c_i}$, $i = 1, \dots, K$
4. $d_k = 1/e_k(\mathbf{p}, v_k)$, $k = 1, \dots, K$
5. Solve the following problem for the current values of v_k and d_k :

$$(\mathcal{P5}) \quad \min_{\mathbf{p} \geq 0} \sum_{i=1}^K d_i e_i(\mathbf{p}, \mathbf{v}_i) \quad (49)$$

$$\text{s.t.} \quad \sum_{i=1}^K p_i \leq P_{\max},$$

6. Update \mathbf{p} by the obtained solution to (49)
 7. **end while**
 8. **Output:** \mathbf{p}^*
-

Algorithm 2 delineates the whole operation for the power allocation. Step 5 includes a subproblem that has to be solved in every iteration. Fortunately, its solution can be obtained in closed-form with $\sqrt{p_k}$, $k = 1, \dots, K$ treated as optimization variables by decomposing the problem into K independent subproblems. In particular, the solution is given by

$$p_k = \min \left(P_{\max}, \frac{q_k d_k^2 v_k^2}{(q_k d_k v_k^2 + \sum_{i=1}^K d_i v_i^2 c_i)^2} \right). \quad (50)$$

Remark 3: The proposed algorithms, i.e., Algorithms 1 and 2 converge quickly and have low computation complexity. Moreover, given that both algorithms achieve a local optimum,

and that the overall algorithm is based on AO, the final solution corresponds to a local optimum, which means that different initializations will result in different solutions, as will be shown below in Sec. VI.

The power allocation presents a similar complexity to the RBM design since similar matrix operations take place in Algorithm 2, i.e., its complexity is $\mathcal{O}(MN^2 + N + M)$.

VI. NUMERICAL RESULTS

In this section, we elaborate on the numerical results concerning the downlink sum SE of RIS-assisted mMIMO systems with channel aging, imperfect CSI, and correlated Rayleigh fading. MC simulations, portrayed by "X" marks, verify our analysis for $n \rightarrow \infty$ even for finite (conventional) system dimensions. This property has been already observed in previous works relying on DE analysis [20], [38], [39]. For the sake of comparison, in certain cases, we also depict the scenarios with MRT precoding, static UEs, and the absence of RIS.

The simulation setup consists of a single cell with radius $R = 1000$ meters. In the center of the cell, there is a BS, which consists of a uniform linear array (ULA) with $M = 100$ antennas that serve $K = 20$ moving UEs while the communication is assisted by an RIS assembled by a uniform planar array (UPA) of $L = 100$ elements. The length of the uplink training duration is $\tau = K$ symbols and the pilot transmit power is $p_p = 6$ dBm. Assuming that the coherence time and bandwidth are $T_c = 2$ ms and $B_c = 100$ kHz, respectively, i.e., the coherence block consists of 200 channel uses. Also, $\sigma^2 = -174 + 10 \log_{10} B_c$. For the sake of exposition, we assume that the temporal correlation coefficient $\alpha_{k,n}$ is the same across all UEs.

The correlation matrices $\mathbf{R}_{\text{BS},k}$ and $\mathbf{R}_{\text{RIS},k}$ are computed according to [38] and [30], respectively. The size of each RIS element, required by the latter, is given by $d_H = d_V = \lambda/4$. In addition, the path-losses corresponding to the BS-to-RIS and RIS-to-UE k links are given by [3], [6]

$$\beta_1 = \frac{C_1}{r_1^{\alpha_1}}, \quad \beta_{2,k} = \frac{C_2}{r_{2,k}^{\alpha_2}}, \quad (51)$$

where α_i and r_i for $i = 1, 2$ are the path-loss exponent and distance for link i . Note that $C_1 = 26$ dB and $C_2 = 28$ dB, which describe the path-losses at a reference distance of 1 m [12]. In the case of the LoS link, we consider the same value for $\beta_{d,k}$ as for $\beta_{2,k}$ but with an additional penetration loss of 15 dB. The choice of these values has been made based on the 3GPP Urban Micro (UMi) scenario from TR36.814 for a carrier frequency of 2 GHz and a noise level of -80 dBm. In particular, the path-losses for links 1 and 2 are generated based on the LOS and NLOS versions [42]. Specifically, we have $\alpha_1 = 2.2$ and $\alpha_2 = 3.67$ while $r_1 = 8$ m and $r_2 = 60$ m. The Doppler spread, corresponding to a relative velocity of 135 km/h between the BS and the UEs, is $f_D = 250$ Hz. Moreover, if we assume that the bandwidth is $W = 20$ MHz, the symbol time is $T_s = 1/(2W) = 0.025$ μ s.

Fig. 2 depicts the relative estimation error per channel element, i.e., the NMSE versus the downlink SNR for different velocities. Certain noise floors appear as $p \rightarrow \infty$. Moreover,

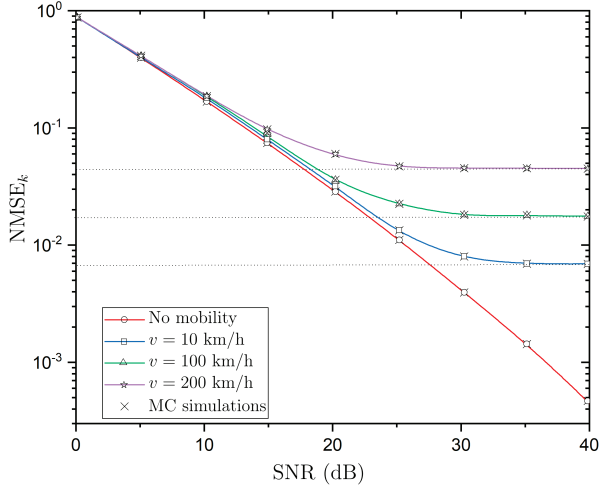


Fig. 2. NMSE of UE k versus the SNR of an RIS-assisted MIMO system with imperfect CSI ($M = 100$, $L = 100$, $K = 20$) for different UE velocities in the cases of uncorrelated fading at the RIS (Analytical results and MC simulations).

we illustrate the result corresponding to no mobility, which decreases without bound. In addition, we observe that the error floors take larger values with increasing mobility (channel aging). It is shown that the NMSE saturates after 25 dB for high velocity while it saturates much later for slow velocity. Note that these results correspond to uncorrelated fading at the RIS to avoid any RBM optimization because, in this case, the NMSE is independent of Θ (Remark 1). However, below, in the case of the sum SE, the optimization with respect to Θ is applied.

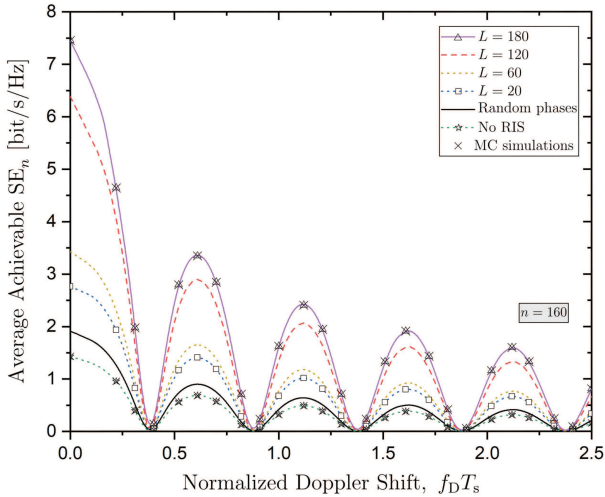


Fig. 3. Downlink achievable sum SE with RZF precoding of an RIS-assisted MIMO system with channel aging versus the normalized Doppler shift $f_D T_s$ for different number of RIS elements L ($M = 100$, $K = 20$) (Analytical results and MC simulations).

In Fig 3, we depict the achievable average SE_n versus the normalized Doppler shift $f_D T_s$ for $n = 160$ while varying the number of RIS elements, i.e., $L = 20, 60, 120, 180$. The ripples are caused because of the dependence from the

correlation coefficient, which takes the form of the Bessel function of zeroth order, i.e., $\alpha_{k,n-K}^2 = J_0^2(2\pi f_D T_s n)$. It is shown that by increasing $f_D T_s$, the average sum SE decreases. An increase in $f_D T_s$ is equivalent to an increase in velocity or duration of the symbol time. Especially, when $f_D T_s \approx 0.39$, the sum rate becomes almost zero for the first time, and then the magnitude fluctuates while tending to zero. Moreover, a larger RIS in terms of number of elements results in larger average sum SE but the curves keep the same shape. Even the zeros of the sum SE appear at the same normalized Doppler shifts. Hence, the presence of a RIS improves the performance even in channel aging conditions.

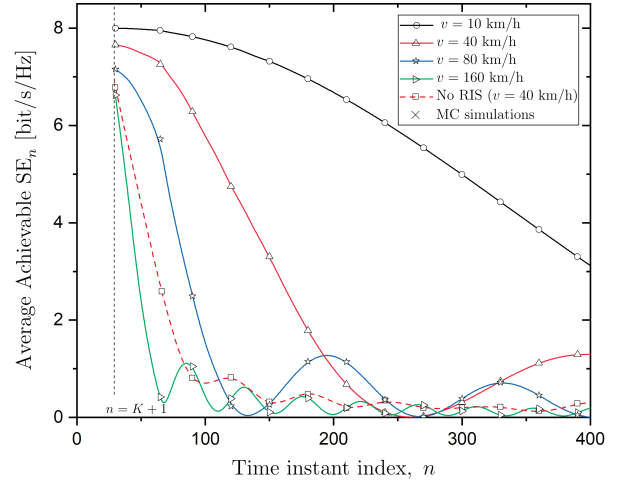


Fig. 4. Downlink achievable sum SE with RZF precoding of an RIS-assisted MIMO system with channel aging versus the time instant index n for different velocities v ($M = 100$, $L = 100$, $K = 20$) (Analytical results and MC simulations).

Fig. 4 shows the achievable average SE_n versus the time instant index n for different UEs velocities. The time index starts at $n = K + 1$, where the data transmission begins. As can be seen, at a given time instant, SE_n decreases with UE mobility. Moreover, as the velocity increases, the first zero position moves to the left, which suggests that the length of coherence time should be designed to account for the impact of channel aging. Also, we depict the scenario with no RIS in the case $v = 40$ km/h, which appears lower SE.

Fig. 5 illustrates the achievable downlink sum \overline{SE} versus the number of RIS elements L for varying UE mobility in terms of the relative velocity v . Obviously, \overline{SE} increases with L as expected, but an increase in velocity degrades the performance. The larger the velocity becomes, the larger the loss in the sum SE is observed. However, an increase with respect to the number of elements still allows for improving the SE despite the degradation due to mobility. Also, we show the results corresponding to static UEs and no RIS that correspond to the horizontal lines, which are parallel to the x -axis. For the sake of further comparison, we illustrate the performance of the simpler MRT precoding under channel aging conditions (dotted lines), which increases with L but is inferior compared to RZF.

Fig. 6 shows also the impact of channel aging in terms of the

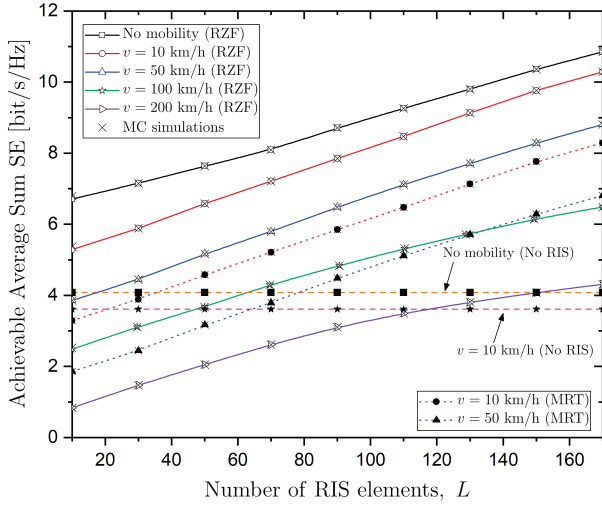


Fig. 5. Downlink achievable sum SE with RZF precoding of an RIS-assisted MIMO system with channel aging versus the number of RIS elements L for different velocities v ($M = 100$, $K = 20$) (Analytical results and MC simulations).

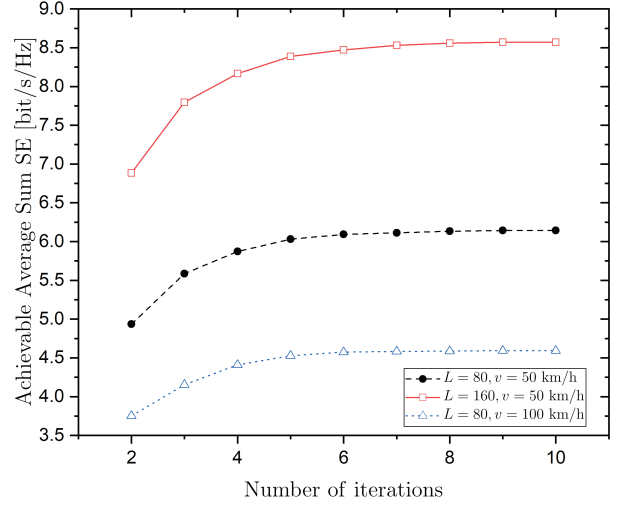


Fig. 7. Downlink achievable sum SE with RZF precoding of an RIS-assisted MIMO system with channel aging versus the number of iterations for different velocities v and number of RIS elements L ($M = 100$, $K = 20$) (Analytical results and MC simulations).

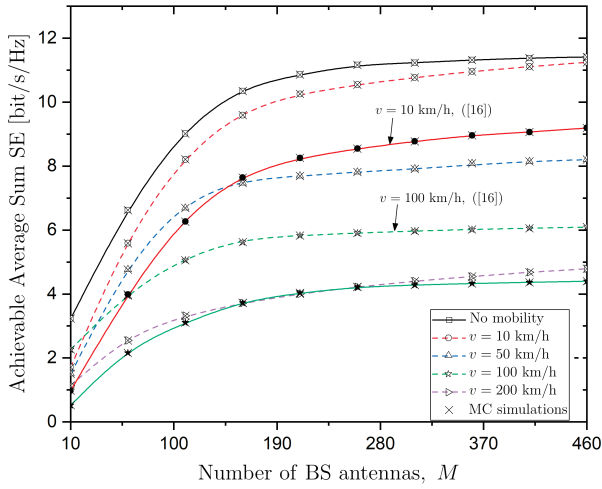


Fig. 6. Downlink achievable sum SE with RZF precoding of an RIS-assisted MIMO system with channel aging versus the number BS antennas M for different velocities v ($L = 100$, $K = 20$) (Analytical results and MC simulations).

achievable sum SE with respect to the number of BS antennas M for different velocities. Generally, the downlink sum rate presents a rise with M . Notably, we observe that when the velocity increases, the sum rate decreases while an increase in the number of BS antennas increases the performance. For the sake of comparison, we have included the solid lines in terms of simulation corresponding to the SE with CE performed according to [16] when $v = 10$ km/h and $v = 100$ km/h. Although the CE in [16] does not account for channel aging, the achievable sum SE is much lower than the proposed method due to its high training overhead.

In Fig. 7, we depict the convergence of the proposed entire algorithm, which is founded on AO and includes the subproblems of RBM and transmit power optimizations. In

particular, the horizontal axis corresponds to the number of iterations. As can be observed, the convergence is achieved quite fast for the cases under study, i.e., about 6 iterations are required. In the same figure, we have shown how the increase in the number of RIS elements and the channel aging affect the convergence. As L increases, more iterations are required to reach convergence because the number of optimization variables is larger. However, channel aging does not affect the rate of convergence but only the rate since the number of optimization variables does not change.

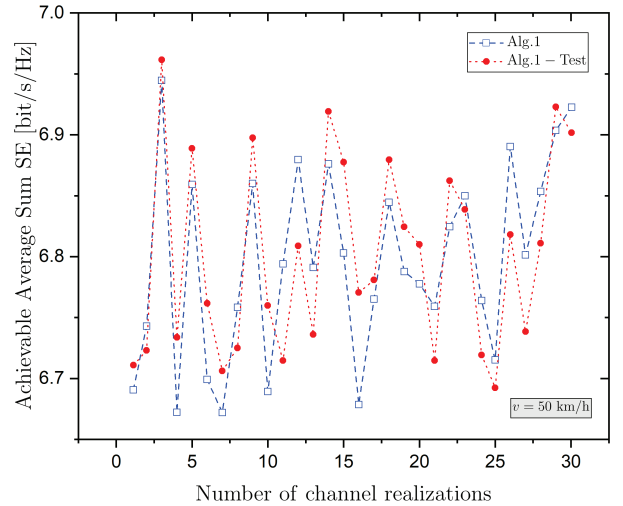


Fig. 8. Downlink achievable sum SE with RZF precoding of an RIS-assisted MIMO system with channel aging versus 30 channel realizations ($M = 100$, $L = 100$, $K = 20$) (Analytical results and MC simulations).

In addition, Fig. 8 assesses the dependence on the choice of the initial points. Specifically, given that the optimization problem 25c is non-convex, its solution is contingent on the initialization. Hence, we consider 30 channel realizations

and $v = 50$ km/h. The overall algorithm, consisted of Algorithms 1 and 2 is initialized with $\mathbf{c}_0 = \exp(j\pi/2)\mathbf{1}_L$ and $\mathbf{p} = \frac{P_{\max}}{K}\mathbf{1}_K$. The line corresponding to "Alg. 1-Test" considers the best initial point out of 100 random initial points for each channel instance. As observed, different initial points lead to different solutions. However, the sum SE in both cases is almost identical, which indicates that the selected initialization regarding the phase shifts and the transmit power is a good choice.

VII. CONCLUSION

In this paper, we studied the impact of channel aging on RIS-assisted mMIMO systems by taking additionally into account the effects of spatial correlation and imperfect CSI. Having introduced channel aging and correlated Rayleigh fading not only during the data transmission phase but also in the uplink training phase, we obtained the effective channel estimates and derived the DE achievable sum SE with RZF in closed form. Next, we provided its maximization with respect to the RIS phase shifts and power budget constraints by applying an efficient AO algorithm based on statistical CSI that reduces both the computational complexity and the feedback overhead. Hence, we illustrated the impact of channel aging and how its interconnection with other fundamental parameters affects performance. For instance, a suitable selection of the number of RIS elements and the length of the frame duration can mitigate channel aging. Notably, this work suggests interesting directions for future research with the study of wideband systems being of prominent significance.

APPENDIX A PROOF OF THEOREM 1

Regarding the term in the desired signal power given by $S_{k,n}$, we have

$$\mathbb{E}\{\mathbf{h}_k^H \mathbf{f}_{k,n}\} = \alpha_{k,n-K} \mathbb{E}\{(\hat{\mathbf{h}}_k^H + \tilde{\mathbf{h}}_k^H) \Sigma_k \hat{\mathbf{h}}_k\} \quad (52)$$

$$\asymp \alpha_{k,n-K} \mathbb{E}\left\{\frac{\hat{\mathbf{h}}_k^H \Sigma_k \hat{\mathbf{h}}_k}{1 + \alpha_{k,n-K}^2 \hat{\mathbf{h}}_k^H \Sigma_k \hat{\mathbf{h}}_k}\right\} \quad (53)$$

$$\asymp \alpha_{k,n-K} \frac{\frac{1}{M} \text{tr}(\Phi_k \mathbf{T})}{1 + \alpha_{k,n-K}^2 \frac{1}{M} \text{tr}(\Phi_k \mathbf{T})} \quad (54)$$

$$= \frac{\alpha_{k,n-K} \delta_k}{1 + \alpha_{k,n-K}^2 \delta_k}, \quad (55)$$

where Σ_k is defined as

$$\Sigma_k = (\alpha_{k,n-K}^2 \hat{\mathbf{H}}_k \hat{\mathbf{H}}_k^H - \alpha_{k,n-K}^2 \hat{\mathbf{h}}_k \hat{\mathbf{h}}_k^H + \mathbf{Z} + \alpha M \mathbf{I}_M)^{-1}.$$

In (53), we have applied the matrix inversion lemma. In (54), we have used [43, Lem. B.26], and [44, Theorem 1]. Also, we have set $\delta_k = \frac{1}{M} \text{tr}(\Phi_k \mathbf{T})$.

For the derivation of the DE of the normalization parameter

λ , we focus on the denominator, and we result in

$$\text{tr}(\mathbf{P} \hat{\mathbf{H}}^H \Sigma^2 \hat{\mathbf{H}}) = \sum_{i=1}^K p_i \hat{\mathbf{h}}_i^H \Sigma^2 \hat{\mathbf{h}}_i \quad (56)$$

$$= \frac{1}{M} \sum_{i=1}^K p_i \frac{\hat{\mathbf{h}}_i^H \Sigma_i^2 \hat{\mathbf{h}}_i}{(1 + \alpha_{i,n-K}^2 \hat{\mathbf{h}}_i^H \Sigma_i \hat{\mathbf{h}}_i)^2} \quad (57)$$

$$\asymp \frac{1}{M} \sum_{i=1}^K p_i \frac{\frac{1}{M} \text{tr}(\Phi_i \tilde{\mathbf{T}}(\mathbf{I}_M))}{(1 + \alpha_{i,n-K}^2 \frac{1}{M} \text{tr}(\Phi_i \mathbf{T}))^2} \quad (58)$$

$$= \frac{1}{M} \sum_{i=1}^K p_i \frac{\delta_i^\lambda}{(1 + \alpha_{i,n-K}^2 \delta_i)^2}, \quad (59)$$

where, in (57), we have applied the matrix inversion lemma twice. In (58), we have applied the rank-1 perturbation lemma, [43, Lem. B.26], and [44, Theorem 1] together with [38, Theorem 2] for $\mathbf{K} = \mathbf{I}_M$. In (59), we have denoted $\delta_i^\lambda = \frac{1}{M} \text{tr}(\Phi_i \tilde{\mathbf{T}}(\mathbf{I}_M))$.

The term in $I_{k,n}$, which includes the deviation from the average effective channel gain is written as

$$\text{Var}\{\mathbf{h}_k^H \mathbf{f}_{k,n}\} \asymp \frac{\alpha_{k,n-K}^2 \mathbb{E}\{|\tilde{\mathbf{h}}_k^H \Sigma_k \hat{\mathbf{h}}_k|^2\}}{(1 + \alpha_{k,n-K}^2 \delta_k)^2} \quad (60)$$

$$\asymp \frac{\alpha_{k,n-K}^2 \text{tr}(\Sigma_k \Phi_k \Sigma_k (\mathbf{R}_k - \Phi_k))}{(1 + \alpha_{k,n-K}^2 \delta_k)^2} \quad (61)$$

$$\asymp \frac{\frac{1}{M^2} \alpha_{k,n-K}^2 \text{tr}((\mathbf{R}_k - \Phi_k) \tilde{\mathbf{T}}(\Phi_k))}{(1 + \alpha_{k,n-K}^2 \delta_k)^2}, \quad (62)$$

where in (60), we have applied the matrix inversion lemma, [43, Lem. B.26], and [44, Theorem 1]. Next step includes application of the rank-1 perturbation lemma, [43, Lem. B.26], and [45, Lem. 10]. and [43, Lem. B.26] again. In (62), we have used [38, Theorem 2].

Similar steps are followed to derive the DE of the term including the innovation error. Specifically, we have

$$\mathbb{E}\{|\tilde{\mathbf{e}}_{k,n}^H \mathbf{f}_{k,n}|^2\} \asymp \frac{\alpha_{k,n-K}^2 \mathbb{E}\{|\tilde{\mathbf{e}}_{k,n}^H \Sigma_k \hat{\mathbf{h}}_k|^2\}}{(1 + \alpha_{k,n-K}^2 \delta_k)^2} \quad (63)$$

$$\asymp \frac{\alpha_{k,n-K}^2 \text{tr}(\Sigma_k \Phi_k \Sigma_k \mathbf{R}_k)}{(1 + \alpha_{k,n-K}^2 \delta_k)^2} \quad (64)$$

$$\asymp \frac{\frac{1}{M^2} \alpha_{k,n-K}^2 \text{tr}(\mathbf{R}_k \tilde{\mathbf{T}}(\Phi_k))}{(1 + \alpha_{k,n-K}^2 \delta_k)^2}. \quad (65)$$

The second term, concerning the multi-user interference, is obtained as

$$\mathbb{E}\{|\mathbf{h}_{k,n}^H \mathbf{f}_{i,n}|^2\} = \alpha_{i,n-K}^2 \mathbb{E}\left\{\left|\frac{\mathbf{h}_{k,n}^H \Sigma_i \hat{\mathbf{h}}_i}{1 + \alpha_{i,n-K}^2 \hat{\mathbf{h}}_i^H \Sigma_i \hat{\mathbf{h}}_i}\right|^2\right\} \quad (66)$$

$$= \alpha_{i,n-K}^2 \mathbb{E}\left\{\frac{\mathbf{h}_{k,n}^H \Sigma_i \hat{\mathbf{h}}_i \hat{\mathbf{h}}_i^H \Sigma_i \mathbf{h}_{k,n}}{(1 + \alpha_{i,n-K}^2 \hat{\mathbf{h}}_i^H \Sigma_i \hat{\mathbf{h}}_i)^2}\right\} \quad (67)$$

$$\asymp \alpha_{i,n-K}^2 \mathbb{E}\left\{\frac{\mathbf{h}_{k,n}^H \Sigma_i \Phi_i \Sigma_i \mathbf{h}_{k,n}}{(1 + \alpha_{i,n-K}^2 \delta_i)^2}\right\}, \quad (68)$$

where the matrix inversion lemma has been applied in (66). In (68), the mutual independence between $\hat{\mathbf{h}}_i$ and $\mathbf{h}_{k,n}$, the rank-1 perturbation lemma, [43, Lem. B.26], and [44, Theorem 1]

are taken into account. However, Σ_i is not independent of $\mathbf{h}_{k,n}$. For this reason, application of [38, Lemma 2] gives

$$\Sigma_i = \Sigma_{ik} - \alpha_{k,n-K}^2 \frac{\Sigma_{ik} \hat{\mathbf{h}}_k \hat{\mathbf{h}}_k^H \Sigma_{ik}}{1 + \alpha_{k,n-K}^2 \hat{\mathbf{h}}_k^H \Sigma_{ik} \hat{\mathbf{h}}_k}, \quad (69)$$

where the new matrix Σ_{ik} is defined as

$$\Sigma_{ik} = (\alpha_{k,n-K}^2 \hat{\mathbf{H}}_k \hat{\mathbf{H}}_k^H - \alpha_{k,n-K}^2 \hat{\mathbf{h}}_k \hat{\mathbf{h}}_k^H - \alpha_{i,n-K}^2 \hat{\mathbf{h}}_i \hat{\mathbf{h}}_i^H + \mathbf{Z} + M\alpha \mathbf{I}_M)^{-1}. \quad (70)$$

By inserting (69) into (68), we result in

$$\mathbb{E}\{|\mathbf{h}_{k,n}^H \mathbf{f}_{i,n}|^2\} = \frac{Q_{ik}}{(1 + \alpha_{i,n-K}^2 \delta_i)^2}, \quad (71)$$

where Q_{ik} is given by (72) at the top of the next page. In (71), we have applied again the matrix inversion lemma, and in the last step, we have used the rank-1 perturbation lemma, [43, Lem. B.26], [44, Theorem 1], and [38, Theorem 2]. The DE of each term in (72) is obtained as

$$\mathbf{h}_{k,n}^H \Sigma_{ik} \Phi_i \Sigma_{ik} \mathbf{h}_{k,n} \asymp \frac{1}{M^2} \text{tr} \mathbf{R}_k \tilde{\mathbf{T}}(\Phi_i) = \zeta_{ki}, \quad (73)$$

$$\hat{\mathbf{h}}_k^H \Sigma_{ik} \Phi_i \Sigma_{ik} \hat{\mathbf{h}}_k \asymp \frac{1}{M^2} \text{tr} \Phi_k \tilde{\mathbf{T}}(\Phi_i) = \mu_{ki}, \quad (74)$$

$$\mathbf{h}_{k,n}^H \Sigma_{ik} \Phi_i \Sigma_{ik} \hat{\mathbf{h}}_k \asymp \alpha_{k,n-K} \frac{1}{M^2} \text{tr} \Phi_k \tilde{\mathbf{T}}(\Phi_i). \quad (75)$$

Hence, substitution of (73)-(75) into (72) provides Q_{ik} .

The definitions of the various parameters are given in the presentation of the theorem. The DE SINR $\tilde{\gamma}_{k,n}$ is obtained by substituting (55), (59), (62), (65), and (71) into $S_{k,n}$ and $I_{k,n}$.

APPENDIX B PROOF OF PROPOSITION 2

For this proof, we are going to use the following lemma.

Lemma 2: Let $\mathbf{A} \in \mathbb{C}^{M \times M}$ be independent of Θ and $\mathbf{R}_k = \mathbf{H}_1 \Theta \mathbf{R}_{\text{IRS},k} \Theta^H \mathbf{H}_1^H$, then

$$\text{tr} \left(\mathbf{A} \frac{\partial \mathbf{R}_k}{\partial \mathbf{c}_t^*} \right) = \mu \text{diag} (\mathbf{H}_1^H \mathbf{A} \mathbf{H}_1 \Theta \mathbf{R}_{\text{IRS},k}). \quad (76)$$

Proof: We have

$$\text{tr} \left(\mathbf{A} \frac{\partial \mathbf{R}_k}{\partial \mathbf{c}_t^*} \right) = \frac{\partial (\text{diag} (\mathbf{H}_1^H \mathbf{A} \mathbf{H}_1 \Theta \mathbf{R}_{\text{IRS},k}))^T \mathbf{c}_t^*}{\partial \mathbf{c}_t^*} \quad (77)$$

$$= \mu \text{diag} (\mathbf{H}_1^H \mathbf{A} \mathbf{H}_1 \Theta \mathbf{R}_{\text{IRS},k}), \quad (78)$$

where we have used the property $\text{tr}(\mathbf{A} \text{diag}(\mathbf{c}_t)) = (\text{diag}(\mathbf{A}))^T \mathbf{c}_t$. ■

The gradient of $\tilde{\gamma}_{k,n}$ with respect to \mathbf{c}_t^* is written as

$$\tilde{\gamma}'_{k,n} = \frac{S'_k I_k - S_k I'_k}{I_k^2}, \quad (79)$$

where the quotient rule derivative was simply applied. We continue with the computation of the partial derivatives S'_k and I'_k . Specifically, S'_g is obtained as

$$S'_k = 2p_k \delta_k \delta'_k, \quad (80)$$

where

$$\delta'_k = \frac{1}{M} \text{tr} (\Phi'_k \mathbf{T} + \Phi_k \mathbf{T}'). \quad (81)$$

Note that Φ'_k is the derivative of Φ_k with respect to \mathbf{c}_t^* whose expression is given by

$$\Phi'_k = \alpha_{k,\zeta-n}^2 (\mathbf{R}'_k \mathbf{Q} \mathbf{R}_k + \mathbf{R}_k \mathbf{Q}' \mathbf{R}_k + \mathbf{R}_k \mathbf{Q} \mathbf{R}'_k). \quad (82)$$

The computation of the trace of this expression requires Lemma 2 and that the derivative of the inverse matrix \mathbf{Q} is obtained according to [46, Eq. 40] as $\mathbf{Q}' = -\mathbf{Q}(\mathbf{Q}^{-1})' \mathbf{Q}$, where the derivative of \mathbf{Q}^{-1} is written as

$$(\mathbf{Q}^{-1})' = \mathbf{R}'_k. \quad (83)$$

Also, \mathbf{T}' concerns the derivative of an inverse matrix written as $\mathbf{T}' = -\mathbf{T}(\mathbf{T}^{-1})' \mathbf{T}$, where the derivative of \mathbf{T}^{-1} is written as

$$(\mathbf{T}^{-1})' = \frac{1}{M} \sum_{i=1}^K \frac{\Phi'_i (1 + \alpha_{i,n-K}^2 \delta_i) - \alpha_{i,n-K}^2 \Phi_i \delta'_i}{(1 + \alpha_{i,n-K}^2 \delta_i)^2}, \quad (84)$$

After inserting (81)-(84) into (80), we obtain S'_k .

The derivative of I_k is based on simple derivative rules and it requires the computation of the derivatives of δ_k , $\tilde{\delta}_k$, δ_k^e , Q_{ik} , and $\bar{\lambda}$ as shown in (30). Regarding δ'_k , it is given by (81), while $\tilde{\delta}'_k$ and $\delta_k^{e'}$ are obtained similarly as

$$\tilde{\delta}'_k = \frac{1}{M} \text{tr} ((\mathbf{R}'_k - \Phi'_k) \tilde{\mathbf{T}}(\Phi_k) + (\mathbf{R}_k - \Phi_k) \tilde{\mathbf{T}}'(\Phi_k)), \quad (85)$$

$$(\delta_k^e)' = \frac{1}{M} \text{tr} (\mathbf{R}'_k \tilde{\mathbf{T}}(\Phi_k) + \mathbf{R}_k \tilde{\mathbf{T}}'(\Phi_k)), \quad (86)$$

where

$$\begin{aligned} \tilde{\mathbf{T}}'(\Phi_k) &= \mathbf{T}' \Phi_k \mathbf{T} + \mathbf{T} \Phi'_k \mathbf{T} + \mathbf{T} \Phi_k \mathbf{T}' \\ &+ \frac{1}{M} \sum_{i=1}^K \frac{\tilde{\delta}'_i \mathbf{T} \Phi_i \mathbf{T} + \tilde{\delta}_i (\mathbf{T}' \Phi_k \mathbf{T} + \mathbf{T} \Phi'_k \mathbf{T} + \mathbf{T} \Phi_k \mathbf{T}')}{(1 + \alpha_{i,n-K}^2 \delta_i)^3} \\ &- \frac{1}{M} \sum_{i=1}^K \frac{2\alpha_{i,n-K}^2 \tilde{\delta}_i \mathbf{T} \Phi_i \mathbf{T} \delta'_i}{(1 + \alpha_{i,n-K}^2 \delta_i)}. \end{aligned} \quad (87)$$

The derivative of the normalization parameter is given by

$$\bar{\lambda}' = \frac{K \left(\frac{1}{M} \text{tr} \left(\frac{\mathbf{Z}}{M} + \alpha \mathbf{I}_M \right) \tilde{\mathbf{T}}'(\mathbf{I}_M) - \frac{1}{M} \text{tr} \mathbf{T}' \right)}{\left(\frac{1}{M} \text{tr} \mathbf{T} - \frac{1}{M} \text{tr} \left(\frac{\mathbf{Z}}{M} + \alpha \mathbf{I}_M \right) \tilde{\mathbf{T}}(\mathbf{I}_M) \right)^2}. \quad (88)$$

Moreover, the last required derivative, concerning Q_{ik} , is obtained as

$$\begin{aligned} Q'_{ik} &= \zeta'_{ki} + \frac{\delta_k \delta'_k \mu_{ki} + |\delta_k|^2 \mu_{ki}}{(1 + \alpha_{k,n-K}^2 \delta_k)^2} + \frac{2\alpha_{k,n-K}^2 |\delta_k|^2 \mu_{ki} \delta'_k}{(1 + \alpha_{k,n-K}^2 \delta_k)^3} \\ &- 2\text{Re} \left\{ \frac{(\delta_k^e)' \mu_{ki} + \delta_k^e \mu'_{ki}}{1 + \alpha_{k,n-K}^2 \delta_k} + \frac{\alpha_{k,n-K}^2 \delta_k^e \mu_{ki} \delta'_k}{(1 + \alpha_{k,n-K}^2 \delta_k)^2} \right\}, \end{aligned} \quad (89)$$

where

$$\zeta'_{ki} = \frac{1}{M^2} \text{tr} (\mathbf{R}'_k \tilde{\mathbf{T}}(\Phi_i) + \mathbf{R}_k \tilde{\mathbf{T}}'(\Phi_i)), \quad (90)$$

$$\mu'_{ki} = \frac{1}{M^2} \text{tr} (\Phi'_k \tilde{\mathbf{T}}(\Phi_i) + \Phi_k \tilde{\mathbf{T}}'(\Phi_i)). \quad (91)$$

Having obtained (85), (86), (88), and (89), the derivative of I_k is derived and the proof is concluded.

$$Q_{ik} = \mathbf{h}_{k,n}^H \boldsymbol{\Sigma}_{ik} \Phi_i \boldsymbol{\Sigma}_{ik} \mathbf{h}_{k,n} + \alpha_{k,n-K}^6 \frac{|\mathbf{h}_{k,n}^H \boldsymbol{\Sigma}_{ik} \hat{\mathbf{h}}_k|^2 \hat{\mathbf{h}}_k^H \boldsymbol{\Sigma}_{ik} \Phi_i \boldsymbol{\Sigma}_{ik} \hat{\mathbf{h}}_k}{(1 + \alpha_{k,n-K}^2 \hat{\mathbf{h}}_k^H \boldsymbol{\Sigma}_{ik} \hat{\mathbf{h}}_k)^2} - 2\alpha_{k,n-K}^4 \operatorname{Re} \left\{ \frac{\hat{\mathbf{h}}_k^H \boldsymbol{\Sigma}_{ik} \mathbf{h}_{k,n} \mathbf{h}_{k,n}^H \boldsymbol{\Sigma}_{ik} \Phi_i \boldsymbol{\Sigma}_{ik} \hat{\mathbf{h}}_k}{1 + \alpha_{k,n-K}^2 \hat{\mathbf{h}}_k^H \boldsymbol{\Sigma}_{ik} \hat{\mathbf{h}}_k} \right\}. \quad (72)$$

REFERENCES

- [1] F. Boccardi *et al.*, “Five disruptive technology directions for 5G,” *IEEE Commun. Mag.*, vol. 52, no. 2, pp. 74–80, 2014.
- [2] E. Basar *et al.*, “Wireless communications through reconfigurable intelligent surfaces,” *IEEE Access*, vol. 7, pp. 116753–116773, 2019.
- [3] Q. Wu and R. Zhang, “Intelligent reflecting surface enhanced wireless network via joint active and passive beamforming,” *IEEE Trans. Wireless Commun.*, vol. 18, no. 11, pp. 5394–5409, 2019.
- [4] C. Pan *et al.*, “Multicell MIMO communications relying on intelligent reflecting surfaces,” *IEEE Trans. Wireless Commun.*, vol. 19, no. 8, pp. 5218–5233, 2020.
- [5] A. Papazafeiropoulos *et al.*, “Intelligent reflecting surface-assisted MIMO systems with imperfect hardware: Channel estimation, beamforming design,” *IEEE Trans. Wireless Commun.*, 2021.
- [6] A. Kammoun *et al.*, “Asymptotic max-min SINR analysis of reconfigurable intelligent surface assisted MISO systems,” *IEEE Trans. Wireless Commun.*, vol. 19, no. 12, pp. 7748–7764, 2020.
- [7] A. Papazafeiropoulos *et al.*, “Asymptotic analysis of Max-Min weighted SINR for IRS-assisted MISO systems with hardware impairments,” *IEEE Wireless Commun. Lett.*, pp. 1–1, 2021.
- [8] A. M. Elbir *et al.*, “Deep channel learning for large intelligent surfaces aided mm-Wave massive MIMO systems,” *IEEE Wireless Commun. Lett.*, vol. 9, no. 9, pp. 1447–1451, 2020.
- [9] H. Guo *et al.*, “Weighted sum-rate maximization for reconfigurable intelligent surface aided wireless networks,” *IEEE Trans. Wireless Commun.*, vol. 19, no. 5, pp. 3064–3076, 2020.
- [10] J. Chen *et al.*, “Intelligent reflecting surface: A programmable wireless environment for physical layer security,” *IEEE Access*, vol. 7, pp. 82599–82612, 2019.
- [11] P. Yang, L. Yang, and S. Wang, “Performance analysis for RIS-Aided Wireless Systems With Imperfect CSI,” *IEEE Wireless Commun. Lett.*, vol. 11, no. 3, pp. 588–592, 2021.
- [12] E. Björnson, Ö. Özdogan, and E. G. Larsson, “Intelligent reflecting surface versus decode-and-forward: How large surfaces are needed to beat relaying?” *IEEE Wireless Commun. Lett.*, vol. 9, no. 2, pp. 244–248, 2019.
- [13] M. Di Renzo *et al.*, “Smart radio environments empowered by reconfigurable intelligent surfaces: How it works, state of research, and the road ahead,” *IEEE J. Sel. Areas Commun.*, vol. 38, no. 11, pp. 2450–2525, 2020.
- [14] D. Mishra and H. Johansson, “Channel estimation and low-complexity beamforming design for passive intelligent surface assisted MISO wireless energy transfer,” in *International Conference on Acoustics, Speech and Signal Processing (ICASSP)*. IEEE, 2019, pp. 4659–4663.
- [15] Z.-Q. He and X. Yuan, “Cascaded channel estimation for large intelligent metasurface assisted massive MIMO,” *IEEE Wireless Commun. Lett.*, vol. 9, no. 2, pp. 210–214, 2019.
- [16] Q. Nadeem *et al.*, “Intelligent reflecting surface-assisted multi-user MISO Communication: Channel estimation and beamforming design,” *IEEE Open J. Commun. Soc.*, vol. 1, pp. 661–680, 2020.
- [17] B. Zheng and R. Zhang, “Intelligent reflecting surface-enhanced OFDM: Channel estimation and reflection optimization,” *IEEE Wireless Commun. Lett.*, vol. 9, no. 4, pp. 518–522, 2019.
- [18] E. Shtaiwi *et al.*, “Channel estimation approach for RIS assisted MIMO systems,” *IEEE Trans. Cogn. Commun. Net.*, vol. 7, no. 2, pp. 452–465, 2021.
- [19] K. Truong and R. Heath, “Effects of channel aging in massive MIMO systems,” *IEEE/KICS J. Commun. Net., Special Issue on massive MIMO*, vol. 15, no. 4, pp. 338–351, Aug 2013.
- [20] A. K. Papazafeiropoulos and T. Ratnarajah, “Deterministic equivalent performance analysis of time-varying massive MIMO systems,” *IEEE Trans. Wireless Commun.*, vol. 14, no. 10, pp. 5795–5809, 2015.
- [21] A. K. Papazafeiropoulos, “Impact of general channel aging conditions on the downlink performance of massive MIMO,” *IEEE Trans. Veh. Tech.*, vol. 66, no. 2, pp. 1428–1442, Feb 2017.
- [22] R. Chopra *et al.*, “Performance analysis of FDD massive MIMO systems under channel aging,” *IEEE Trans. Wireless Commun.*, vol. 17, no. 2, pp. 1094–1108, 2017.
- [23] Y. Chen, Y. Wang, and L. Jiao, “Robust transmission for reconfigurable intelligent surface aided millimeter wave vehicular communications with statistical CSI,” *IEEE Trans. Wireless Commun.*, pp. 1–1, 2021.
- [24] M.-M. Zhao *et al.*, “Intelligent reflecting surface enhanced wireless network: Two-timescale beamforming optimization,” *IEEE Trans. Wireless Commun.*, vol. 19, no. 8, pp. 5218–5233, 2020.
- [25] T. Van Chien *et al.*, “Outage probability analysis of IRS-assisted systems under spatially correlated channels,” *IEEE Wireless Commun. Lett.*, pp. 1–1, 2021.
- [26] A. Papazafeiropoulos *et al.*, “Coverage probability of distributed IRS systems under spatially correlated channels,” *IEEE Wireless Commun. Lett.*, pp. 1–1.
- [27] L. You *et al.*, “Reconfigurable intelligent surfaces-assisted multiuser MIMO Uplink Transmission With Partial CSI,” *IEEE Trans. Wireless Commun.*, vol. 20, no. 9, pp. 5613–5627, 2021.
- [28] K. Zhi *et al.*, “Power scaling law analysis and phase shift optimization of RIS-Aided Massive MIMO Systems With Statistical CSI,” *IEEE Trans. Commun.*, vol. 70, no. 5, pp. 3558–3574, 2022.
- [29] Y. Zhang *et al.*, “Performance analysis of reconfigurable intelligent surface assisted systems under channel aging,” *Intelligent and Converged Networks*, vol. 3, no. 1, pp. 74–85, 2022.
- [30] E. Björnson and L. Sanguinetti, “Rayleigh fading modeling and channel hardening for reconfigurable intelligent surfaces,” *IEEE Wireless Commun. Lett.*, vol. 10, no. 4, pp. 830–834, 2021.
- [31] D. Neumann, M. Joham, and W. Utschick, “Covariance matrix estimation in massive MIMO,” *IEEE Signal Process. Lett.*, vol. 25, no. 6, pp. 863–867, 2018.
- [32] S. Abeywickrama *et al.*, “Intelligent reflecting surface: Practical phase shift model and beamforming optimization,” *IEEE Trans. Commun.*, vol. 68, no. 9, pp. 5849–5863.
- [33] E. Björnson, J. Hoydis, and L. Sanguinetti, “Massive MIMO networks: Spectral, energy, and hardware efficiency,” *Foundations and Trends® in Signal Processing*, vol. 11, no. 3–4, pp. 154–655, 2017.
- [34] B. Hassibi and B. Hochwald, “How much training is needed in multiple-antenna wireless links?” *IEEE Trans. Inform. Theory*, vol. 49, no. 4, pp. 951–963, April 2003.
- [35] M. Medard, “The effect upon channel capacity in wireless communications of perfect and imperfect knowledge of the channel,” *IEEE Trans. Inf. Theory*, vol. 46, no. 3, pp. 933–946, May 2000.
- [36] E. Björnson, M. Matthaiou, and M. Debbah, “Massive MIMO with non-ideal arbitrary arrays: Hardware scaling laws and circuit-aware design,” *IEEE Trans. Wireless Commun.*, vol. 14, no. 8, pp. 4353–4368, Aug 2015.
- [37] A. Pitarokoilis, S. Mohammed, and E. Larsson, “Uplink performance of time-reversal MRC in massive MIMO systems subject to phase noise,” *IEEE Trans. Wireless Commun.*, vol. 14, no. 2, pp. 711–723, Feb 2015.
- [38] J. Hoydis, S. ten Brink, and M. Debbah, “Massive MIMO in the UL/DL of cellular networks: How many antennas do we need?” *IEEE J. Select. Areas Commun.*, vol. 31, no. 2, pp. 160–171, February 2013.
- [39] R. Couillet and M. Debbah, *Random matrix methods for wireless communications*. Cambridge University Press, 2011.
- [40] S. Boyd, S. P. Boyd, and L. Vandenberghe, *Convex optimization*. Cambridge university press, 2004.
- [41] Q. Shi *et al.*, “An iteratively weighted MMSE approach to distributed sum-utility maximization for a MIMO interfering broadcast channel,” vol. 59, no. 9, pp. 4331–4340, 2011.
- [42] E. Access, “Further advancements for E-UTRA physical layer aspects,” *3GPP Technical Specification TR*, vol. 36, p. V2, 2010.
- [43] Z. Bai and J. W. Silverstein, *Spectral analysis of large dimensional random matrices*. Springer, 2010, vol. 20.
- [44] S. Wagner *et al.*, “Large system analysis of linear precoding in correlated MISO broadcast channels under limited feedback,” *IEEE Trans. Inf. Theory*, vol. 58, no. 7, pp. 4509–4537, July 2012.
- [45] R. Krishnan *et al.*, “Linear massive MIMO precoders in the presence of phase noise-A large-scale analysis,” *IEEE Trans. Veh. Tech.*, vol. 65, no. 5, pp. 3057–3071, 2016.
- [46] K. B. Petersen and M. S. Pedersen, “The matrix cookbook, nov 2012,” URL <http://www2.imm.dtu.dk/pubdb/p.php>, vol. 3274, p. 14, 2012.